Modellering av en LNG fordons tank med hänsyn till realtidsimplementation

CHRISTIAN WESSEL

KTH Industrial Engineering
and Management

Examensarbete
Stockholm, Sverige Juni 2015

MMK-2015:74 MDA:513

Modeling of a vehicular LNG tank with regard to real time implementation

CHRISTIAN WESSEL

KTH Industrial Engineering
and Management

Master's Degree Project
Stockholm, Sweden June 2015

MMK-2015:74 MDA:513

KTH Industriell teknik och management

Examensarbete MMK 2015:74 MDA 513

Modellering av en LNG fordons tank med hänsyn till realtidsimplementation

Christian Wessel

Godkänt	Examinator	Handledare
2015-06-22	Martin Törngren	Bengt Eriksson
	Uppdragsgivare	Kontaktperson
	Scania CV AB	Svante Löthgren

Sammanfattning

Användningen av naturgas (NG) som ett alternativt fordonsbränsle blir allt mer vanligt. På grund av en faktor på cirka 600 mellan densiteten hos vätske- och gasfas, är det önskvärt att lagra flytande naturgas (LNG) i kryotankar, för användning i naturgasdriven tung trafik. LNG är ett nytt koncept på fordonsmarknaden, vilket förklarar varför det finns lite forskning inom området ”modellering av LNG-fordonstankar”. Målet med detta examensarbete är att utvidga denna forskning, genom att utveckla en modell av en LNG-fordonstank, med en ny modelleringsstrategi, som nyttjar mättnadsegenskaperna hos metan. Den modell som utvecklats i avhandlingen är tänkt att kunna användas i ett inbyggt system, för exempelvis fordonsdiagnostik kopplat till LNG. Hänsyn till detta har därför tagits under modellutveckling och modellen kan överföras till ett inbyggt system och realiseras med låg resurs användning. Dessutom utvärderas användningen av ett Extended Kalman Filter (EKF) som en observatör i LNG-tankmodellen, med slutsatsen att användningen är möjlig.

Modellen har validerats för dynamiska fall mot mätdata erhållen från mätningar i ett tungt fordon med ett LNG-tanksystem i drift som förväntas för fordon med LNG som bränsle. För stationära fall har modellen validerats mot data från tanktillverkaren. Resultatet avhandlingen pressenterar visar att god estimering av tankens tillstånd kan uppnås med en relativt enkel modell. Resultatet visar även modellens okänslighet mot parameterestimering i dynamiska fall medans känsligheten är proportionell mot estimeringen av LNG-tankens isoleringsförmåga, i det stationära fallet.

KTH Industrial Engineering and Management

Master of Science Thesis MMK 2015:74 MDA 513

Modeling of a vehicular LNG tank with regard to real time implementation

Christian Wessel

Approved	Examiner	Supervisor
2015-06-22	Martin Törngren	Bengt Eriksson
	Commissioner	Contact person
	Scania CV AB	Svante Löthgren

Abstract

The usage of natural gas (NG) as an alternative vehicle fuel is becoming more and more common, due to a factor of approximately 600 between the liquid and vapour phase density, the storage of liquefied natural gas (LNG) in cryogenic containers is desirable to enable for NG propelled long haulage vehicles. Due to the novelty of the LNG vehicular market, little research in the field “modeling of LNG vehicular tanks” exists. It is the aim of this Master thesis to add to this research, by developing a model of a vehicular LNG tank, with a new modeling strategy, using the saturation properties of methane. The model developed in the thesis is intended to be used in an embedded system, in one example for vehicular diagnosis related to LNG. Therefore consideration to implementation has been taken during the model development and the model can be realized in an embedded system with low usage of resources. Furthermore the usage of an Extended Kalman Filter (EKF) as an LNG tank model observer is evaluated in the thesis and concluded to be applicable.

The model has been validated in dynamic operation against measurement data obtained from measurements in a heavy vehicle with a LNG tank system. In operating conditions expected from vehicles with LNG as propulsion fuel. For stationary operation the model has been validated against data from the tank manufacturer. The thesis result shows that the model states can be estimated with satisfactory accuracy, with a relative simple model. Furthermore the result show the models low sensitivity to parameter estimation in dynamic operation and proportional sensitivity to the estimation of the LNG tanks isolation ability, in stationary operation.

Contents

List of Figures

List of Tables

Chapter 1

Introduction

In this Chapter the background to the problem to be solved in the Master thesis is presented, the purpose, the restrictions of the thesis and the research questions that the thesis should answer are also presented.

1.1 Background

A model of a vehicular LNG tank has been developed in this Master thesis. This is needed for several reasons and these are covered in this section.

1.1.1 Natural Gas

The usage of alternative fuels in vehicle applications are due to emission legislation and customer demand of lower fuel economy a desirable replacement to conventional fuels such as gasoline and diesel [8]. Two promising candidates to meet thees requirements are natural gas and bio-gas. Natural gas (NG) is the second largest alternative fuel in the world [9], a fossil fuel but since it's main component is methane [10], which with its simple molecular structure CH_4, makes it a inherently clean-burning fuel. Resulting in low particle emissions, low toxicity exhaust gases [9] and less NO_x [8] than conventional fuels. This fact alone makes NG a desirable vehicle fuel in today's market, heavily regulated against emissions. Since natural gas is a rest product in oil extraction and there exist huge natural gas reservoirs around the world. The available supply is colossal, while the demand in comparison is small. Therefor the price of natural gas when not heavily taxed, is very low compared to oil based fuels such as gasoline and diesel [8].

1.1.2 Bio Gas

Bio-gas main component is also methane and it's physic-chemical properties are nearly identical to natural gas [8]. Despite of this it has no effect on global warming since it in the end is made from, among others, the decomposition of plants which has bounded atmospheric CO_2 during its life time, bio-gas is often considered a carbon-neutral fuel. In fact under certain comparisons with a diesel powered Heavy Goods

Vehicle, the gCO_2/km is negative [11]. According to the comparison made in [11] when considering the complete production chain of Bio-gas, Bio-gas powered vehicles only emit 15% of the greenhouse gas emitted by vehicles powered by gasoline and diesel. Also the lower the tax imposed on the fuel, the greater the economic advantages for both consumer and producer [11]. The combustion cycle in a vehicle application of bio-gas or Natural gas is the same, but the general term used in industry refer to Natural gas since this is most common. This terminology will also be used from here on out in this thesis.

1.1.3 Natural gas vehicle market

Because of thees reasons the Natural Gas Vehicle market is constantly expanding, in 2014 the number of Natural Gas Vehicles (NGV) worldwide was 17 730 433 according to the Natural & bio Gas Vehicle Association (NGVA). There are two ways to store natural gas in vehicular fuel storage applications, as Compressed Natural Gas (CNG) or as Liquefied Natural Gas (LNG). Vehicles with CNG storage have a vast majority of the NGV market, but due to the limited range of CNG propelled NGV and a factor of about 630 between CNG and LNG density at atmospheric pressure [8]. LNG vehicles are desirable for long haulage and heavy duty truck applications. An indicative comparison [8] show that the range for a truck propelled by LNG is 160 km for 100 l of fuel and 63 km for CNG. Meaning that the performance of an LNG truck can compete with that of a diesel, which had a range of 270 km in the comparison above. Combined with the economical and environmental advantages described earlier, LNG is a desirable and sustainable fuel storage solution, for the heavy duty trucks of the future.

1.1.4 Natural gas vehichle storage

In CNG systems natural gas, as the name suggest, is stored under 200 bar pressure in metallic or composite tanks [12]. While LNG is stored in super insulated cryogenic containers to keep it in it's liquid form [13]. Since the main component of LNG is methane which has a boiling point of -162 at atmospheric pressure [2] and vehicular LNG tanks using passive cooling systems to enable the vehicle to be stationary. The complexity of the cryogenic vehicular containers is high [13]. Due to the large temperature difference between ambient temperatures and the temperature required to keep LNG in its liquid form. LNG storage containers use a so called super insulation [13],[6],[4],[14], to minimize the heat transferred from the outside environment to the LNG inside the tank.

Although being small, the heat that reach the cryogenic LNG tank is absorbed according to the first law of thermodynamics by the closed system, increasing the system energy by raising the pressure and temperature. Since generally the cryogenic storage tanks are not designed for high pressure operation, a way to vent part of the vapour phase is required for all LNG tanks [15], to reduce the tank pressure and prevent the tank from rupturing when stationary for a long time. The ECE R110

legislation therefore specify that all tanks operating in the EU must have a pressure relive solution and a hold time at the tank suppliers optimal filling point of at least 5 days during stationary operation [15]. I.e. the tank must be able to be stationary without venting any of its gas phase for 5 days after being filled. The rupture of an LNG tank is very dangerous since when the cryogenic liquid comes in contact with the ambient environment it causes an Boiling Liquid Expanding Vapour Explosion (BLEVE) with a destructive radius of up to 257 m [16]. Combined with the fact that NG is flammable under certain mixtures in air, the rupture of an LNG tank is a recipe for disaster.

1.1.5 Composition of LNG

LNG typically has a higher fraction of methane than CNG due to the liquefaction process [17] witch also removes the CO_2 which is an inert gas for the engine, affecting the combustion. The difference between the methane fraction is for a generic NG composition, 84% methane for CNG and 95% for LNG [17]. Except for methane, LNG typically also consist of ethane, propane, butane and sometimes nitrogen. A typical composition of LNG is methane 93.32%, ethane 4.65%, propane 0.84%, butane 0.18% and nitrogen 1.01% [10]. Generally however the composition of NG varies a lot over the world, more so for CNG than LNG. An example of the variations of LNG compositions are shown below in Table 1.1.

Table 1.1: LNG compositions at different geographic locations [5]

Source	Methane	Ethane	Propane	Butane	Nitrogen
Alaska	99.72	0.06	0.0005	0.0005	0.20
Algeria	86.98	9.35	2.33	0.63	0.71
Baltimore Gas & Electric	93.32	4.65	0.84	0.18	1.01
New York City	98.00	1.40	0.40	0.10	0.10
Sand Diego Gas & Electric	92.00	6.00	1.00	-	1.00

The great variation in the composition of NG affect the engine combustion, fuel economy and emissions [18], however due to the many components in the gas it is very hard to determine the exact composition of the NG in the vehicular tank. This is because the determination of an exact composition require one gas quality sensor per component in the gas. Theses gas quality sensors are also expensive, making the incentive to implement such a solution in a vehicle application low. Instead other adaption solutions are used in CNG systems today, often with some deviation from a 100% methane composition. The purer compositions of LNG as compared to CNG will most likely have an even lower incetive to implement an expensive gas quality sensor solution.

1.1.6 Embedded system limitations

An embedded micro controller is more limited in computing power than a computer. In most cases and in this one the processor of the embedded system, considered in the thesis, must not be locked in computation of a model, since this will hinder it from performing safety critical tasks. Due to the complexity of the process in the tank, a model of it will most likely require heavy calculations if the limitations of the embedded system is not considered during the modeling. Furthermore adding more sensors to a system can reduce required calculations of system states but adds to the production cost of it.

1.2 Purpose and definitions

The purpose of the Master thesis is to, with the introduction of vehicular LNG tank systems, create a model of the tank as an implementation prof of concept and for simulation in a computer environment. The model will ultimately be implemented on an embedded system to be used for diagnosis, for future control of the tank pressure. Therefore a mechatronic mindset needs to be applied on each step of the modeling i.e. consider such things as sensors limitations, usage of memory, computational time, sample time e.t.c. So that the translation from computer to embedded system is possible.

1.2.1 Restrictions

The following restrictions should be applied:

- An LNG tank without active cooling should be modelled.
- The model should be translatable to a Scania Electronic control unit (ECU) and run on it during vehicle operation.
- The amount of sensors required for model operation should be kept to a minimum to avoid increased production cost of a NGV with an ECU model implementation.
- The computer model should be developed in MATLAB/Simulink.
- The computer model should be verified against measurements on an LNG truck provided by Scania.
- The model should be physically parameterized allowing for proper model operation, regardless of the types of components in the tank system.

1.2.2 Research questions

The research questions this Master thesis should answer are the following:

1. What are the most important factors to consider when modeling the process in an LNG tank, on a computer, but intended to run on an embedded system with lower computing power performance, operating in a vehicle application? What model accuracy can be achieved?

2. What is the best implementation strategy to be able to translate the computer model to an embedded system with considerable less computing power. What is the minimum amount of sensors and computing power required so that the model can be used for the intended application?

3. Investigation of the possibility's on the current system:

   (a) What sensors are possible to use?

   (b) What sensor placement is possible? In tank, on piping, in gas delivery system?

   (c) What observers can be used, without locking the processor loop? Dynamical or static?

4. What calculation time of the model can be achieved on a modern Embedded system processor [7], with 80 MHz clock frequency when using fixed points? Can a model of a complex cryogenic system processor load be under 1 %?

1.3 Methodology

The overall approach of the thesis to answer the research questions is first through a literature study to identify the most important factors to consider when modeling a vehicular LNG tank, tanking into account that the modeling computation must not require to much resources on an embedded micro controller, but still so enough accuracy is achieved. Furthermore when the choice of modeling strategy is chosen, consideration to implementation viability will be taken so that the model built in MATLAB/Simulink [3] is possible to move to an embedded system. During the design of the model the available sensors in the system must be identified and evaluated so that the model can be designed to use a minimum amount of sensors, in accordance with the restrictions of the thesis in section 1.2.1. Once the model strategy has been chosen and the model has been built in MATLAB/Simulink [3], measurements from a Scania LNG truck will be used to verify the model through simulation by supplying the model with the same input as the real tank in the measurement. Furthermore the hold time of the tank model will be simulated and verified against indicative data provided by the tank manufacturer. Once the model is verified, the computational time and the processor load of the developed model will be analysed, together with an observer solution in the form of an extended Kalman filter, that will be tested on the model and evaluated, both with respect to performance and processor load.

1.4 Report outline

1. Chapter 1: Description of the background of the Master thesis, the purpose and the research questions the thesis should answer.

2. Chapter 2: Description of the physical process inside the LNG tank, both from a modeling perspective and the phenomenons in a real LNG tank.

3. Chapter 3: Description of the vehicular LNG tank that is modeled in the thesis, the operation modes of the tank and the sensors of the system is identified.

4. Chapter 4: Description of the choice of modeling strategy chosen for the model developed in the thesis and presentation of that model.

5. Chapter 5: Description of other research related to the modeling of LNG tanks, evaluation of that research viability in the application of the thesis, description of the model implementation in MATLAB/Simulink [3], verification of the model presented in Chapter 4 through simulation, description of the extended Kalman filter and evaluation of the performance of the filter.

6. Chapter 6: Analysis of the required resources of the developed model, alternative implementation strategies and extended Kalman filter. General conclusions, improvements of the developed material, analysis of possible sensor placement in the system and the answering of the research questions.

Chapter 2

LNG Physics

In this chapter the physical properties of LNG inside an cryogenic container is explained both as they occur in reality and how they can be viewed from a modeling perspective. At the end the assumptions used in the modeling are presented.

2.1 Saturated system and Phase transition

As mentioned in Section 1.1.1 the main component of LNG is methane and its phase properties are shown in Figure 2-1. Here the saturation properties can be seen as the thick lines, left is the liquid properties and the right is vapour. The region inside the saturation lines is sometimes referred to as the "Vapour dome" [19]. Every point inside the Vapour dome represent an equilibrium state for which pure liquid and vapour phase can co-exist under a given *saturation pressure* and *saturation temperature* [19]. I.e. at equilibrium, for every *saturation pressure* both vapour and liquid have the same *saturation temperature* and there exist a clear boundary between the two phases. Naturally in a confined space with the vapour phase above the liquid, such as a cryogenic LNG tank, this boundary is the liquid surface. In the scope of this thesis a saturated system is defined as; a system which state space consist only of that inside the Vapour dome. I.e it is hence assumed in a saturated system that the *complete system does not* assumes pure liquid or pure vapour phase and is never sub coled or super heated hence the saturated system states will remain inside the Vapour dome at all times.

Every horizontal line through the Vapour dome represent a *saturation pressure* and a *saturation temperature*. Every point on this line represent a mixture equilibrium state between liquid and vapour phase, with 100 % vapour at the vapour saturation line boundary and 0 % vapour (100 % liquid) at the saturated liquid line. Seen as x in Figure 2-1. However the state space inside the vapour dome is only to be used for the mixture of the phases when viewing the *complete system* as a whole. I.e. when determining the properties of the complete mixture. This means that for every mixture equilibrium point on a horizontal line through the Vapor dome, the liquid phase of the mixture will have the properties of the point precisely on the saturated

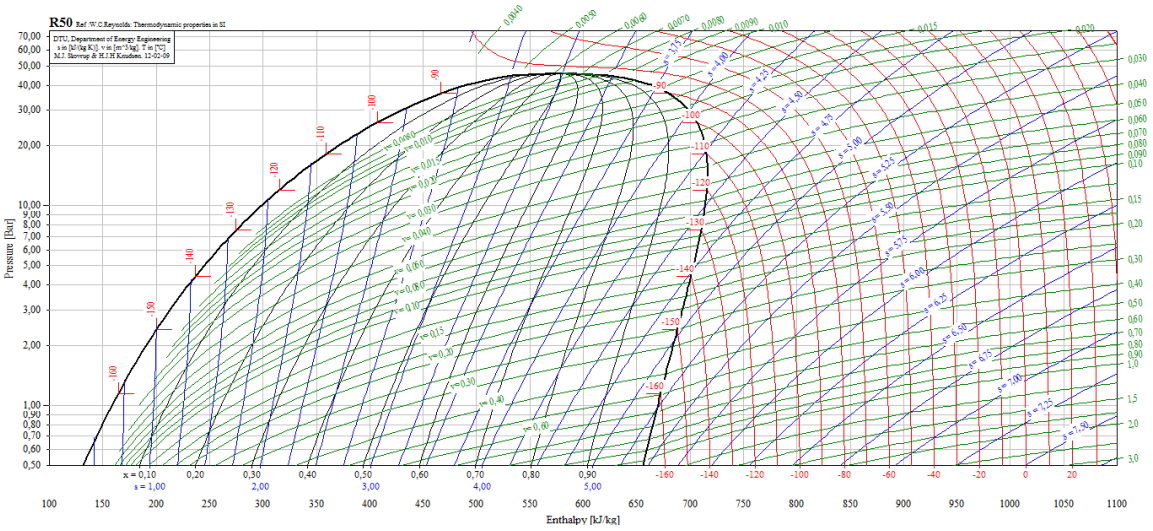

Figure 2-1: Methane phase diagram with p in $log(Bar)$, h in kJ/kg. Lines: Red; T in ^oC, Green; $v = 1/\rho$ in m^3/kg, Black; mass fraction $x = m_g/(m_l + m_g)$ [1].

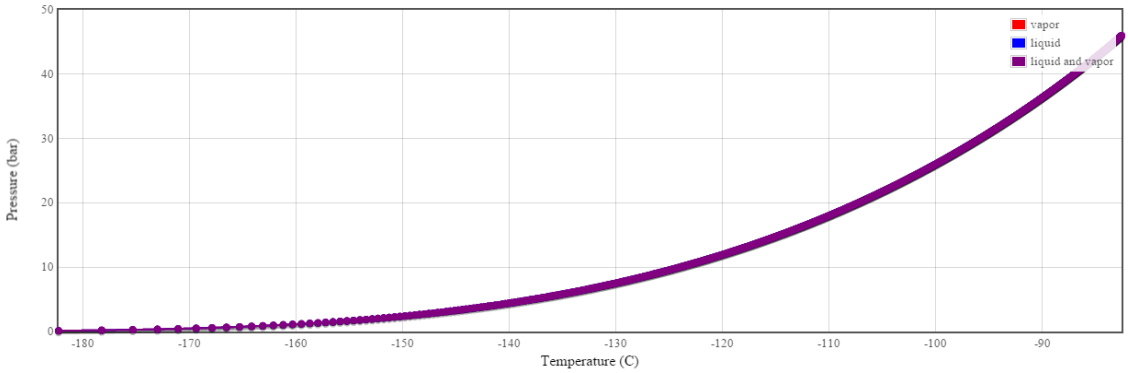

Figure 2-2: One-to-one correspondence between p in Bar and T in ^oC [2].

liquid line and the vapour phase those of the point on the saturated vapour line. From a modeling perspective this means that keeping track of the vapour and liquid mass and handling the liquid and vapour phase separately in equations. The properties of the two phases can be derived at each saturation line for the whole state space.

There is a one-to-one correspondence between the saturation pressure and temperature [19] seen in Figure 2-2. From here on and through out the thesis, a reference to a saturation pressure hence also implies one to a saturation temperature and vice versa. The saturation temperature can be interpreted as the boiling point of a the liquid phase at a given pressure. Furthermore, given the phase properties evaluation at the saturation lines, the terminology liquid and vapour phase and saturated liquid and vapour phase refers to the phase evaluated at its saturation line. If not otherwise specified, the pressures presented in the thesis are absolute, i.e. relative to vacuum.

2.1.1 System energy absorption

If no energy is added to or extracted from the system, the liquid and vapour phase will stay in the initial equilibrium point on their respective saturation line indefinitely. However, changing the system energy will move the liquid and vapour phase along the saturation lines, to a new equilibrium. A phase transition occurs under constant pressure and temperature and moves a portion of the transitioning phase along the horizontal lines through the Vapour dome. From the saturated liquid line to the saturated vapour line, for evaporation, which require energy. Or from the saturated vapor line to the saturated liquid line, for condensation, which reject energy. The energy consumed or released during a phase transition is called the latent heat of vaporisation L_v and is defined as the difference in enthalpy between the saturated vapour phase h_g and the saturated liquid phase h_l [20] at a given saturation temperature as in equation 2.1.

$$L_v(T) = h_g(T) - h_l(T) \tag{2.1}$$

Where the subscripts g and l represent vapour (gas) and liquid respectively. Studies have shown [13] that the phase transition take place solely at the boundary between the two phases, i.e. by surface evaporation and condensation.

The phase transitions through the vapour dome can be described with the same equation only by changing the sign. The heat flux $\dot{Q}_{vap}$ required to evaporate $\dot{m}_{vap}$ of LNG is [20][4]

$$\dot{Q}_{vap} = L_v(T)\dot{m}_{vap}, \tag{2.2}$$

The heat flux released by condensation is defined as

$$\dot{Q}_{cond} = L_v(T)\dot{m}_{cond} \tag{2.3}$$

where $\dot{m}_{cond}$ is the mass flow due to condensation. For simplification of further equations the phase transition heat flux is defined as the difference between the energies in equation 2.2 and 2.3,

$$\dot{Q}_{phase} = L_v(T)(\dot{m}_{vap} - \dot{m}_{cond}) = L_v(T)\dot{m}_{BOG}. \tag{2.4}$$

Where the subscript abbreviation BOG refer to Boil-Off Gas, which is the generally used term in the cryogenic container field [13], but here $\dot{m}_{BOG}$ is defined as the mass transfer between the phases. Hence, $\dot{Q}_{phase} > 0$ and $\dot{m}_{BOG} > 0$ represent evaporation and $\dot{Q}_{phase} < 0$ and $\dot{m}_{BOG} < 0$ represent condensation. The phase transition heat flux give rise to a pressure rise or fall, i.e. an increase or decrease in the system kinetic energy. This represent a move in the vertical component of the saturation lines in Figure 2-1.

Time differentiating the general heat energy equation for any generic substance at a given temperature [21], under the assumption that vapour and liquid have the same temperature in the saturated system. The total heat flux absorption ability of

both the liquid and vapour phase is obtained as

$$\dot{Q}_{heat} = (c_{pg} m_g + c_{pl} m_l)\dot{T}. \tag{2.5}$$

Where c_{pg} and c_{pl} are the heat capacities of each phase, m_g and m_l the mass of each phase and $\dot{T}$ is the temperature time derivative. The heat flux due to the heating of the phases represent an increase in the system thermal energy. This represent a move in the horizontal component of the saturation lines in Figure 2-1. The thermal resistance of the system is from equation 2.5 defined as

$$R = c_{pg} m_g + c_{pl} m_l. \tag{2.6}$$

Note that the heat capacities c_p in equation 2.6 is approximately constant in the Vapour dome state space, except for close to the critical pressure and temperature [2] and can therefore be modeled as mean value constants. The heat fluxes in equations 2.4 and 2.5 are the two forms of absorbing energy supplied to the cryogenic system and hence the driving factors moving the system states to a new phase equilibrium along the saturation lines.

2.1.2 Heat in leak

The heat transfer between the ambient environment and the cryogenic system inside an LNG tank is in reality a complex process as described in section 2.2. However, using a one dimensional linear heat transfer model from [22]. All the heat transfer coefficients for each transfer stage, from ambient to the cryogenic liquid and vapour, can be super positioned into one constant C. The heat flux $\dot{Q}_{in}$ between the ambient temperature T_{amb} and the tank temperature T is hence [4]

$$\dot{Q}_{in} = C(T_{amb} - T). \tag{2.7}$$

Note that the heat flux in equation 2.7 is always positive since the relation $T_{amb} > T$ is always true, for any reasonable operation mode of the cryogenic tank. I.e. there is always a positive heat flux into the tank, except when $T_{amb} = T$. The energy aggregated from this uni-directional heat flow is hence always added to the saturated system energy moving it up the saturation lines. The only way to decrease the energy of a passively cooled cryogenic tank system, is hence to remove mass from it by venting or by fuel delivery to the engine. By fueling the tank with LNG with a lower temperature than the vehicular tank temperature, the saturated system is forced to a lower equilibrium on the saturation lines. I.e. it is in these ways the temperature of a passively cooled cryogenic container is maintained at cryogenic levels. Note that a negative value of $\dot{Q}_{phase}$ in equation 2.4 does *not* mean rejection of energy from the tank, but instead a heat release to be absorbed by $\dot{Q}_{heat}$ in equation 2.5. All energy supplied to the system according to equation 2.7 is hence bound by the system.

2.1.3 Pressure variations in the tank

The liquid phase can be considered incompressible and due to the relative small dimensions in a vehicle tank the hydrostatic pressure can be neglected [22]. Hence the pressure on the liquid phase is the vapour pressure, which agrees with the definition of a saturated system above. When heat continuously is supplied to the saturated system, the pressure and temperate of the system increases and the states are moved upward along the saturation lines in Figure 2-1. The pressure is increased due to the evaporated liquid mass $\dot{m}_{vap}$ in equation 2.2, entering the vapour space and due to the liquid compressing the vapour space. This since the density of the liquid is decreased quite aggressively with a rising temperature, seen in Figure 2-3. The decrease in density is an increase of the liquid volume V_l which, due to the liquid being incompressible, compresses the vapour, raising the pressure in the tank. Note that if the pressure rise due to liquid compression of the vapour space is not in equilibrium with the system temperature rise, $\dot{Q}_{phase} < 0$ in equation 2.4, i.e. vapour mass is condensed and energy rejected from $\dot{Q}_{phase}$ to $\dot{Q}_{heat}$ in equation 2.5 until the system reaches a pressure-temperature equilibrium.

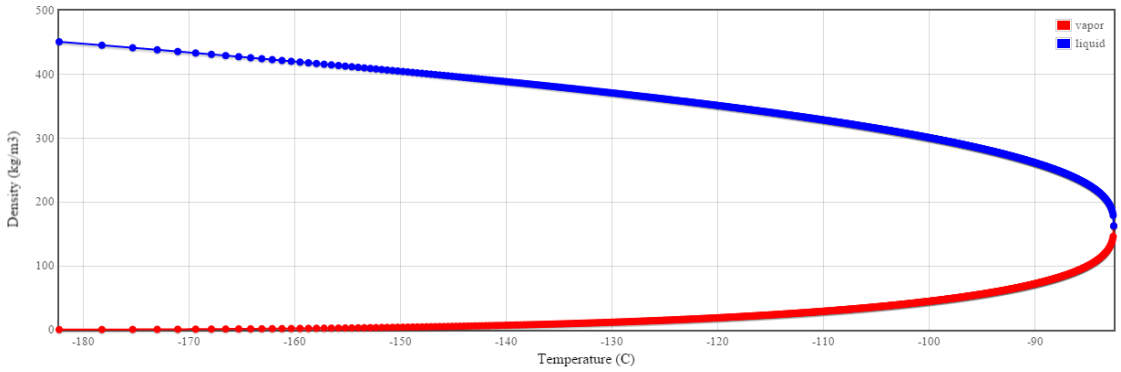

Figure 2-3: Saturation properties between density ρ in kg/m^3 and temperature T in ^oC [2].

Removing mass from the cryogenic tank system lowers the pressure of the tank by vapour expansion in two different ways. Removing liquid mass reduces the liquid volume, enabling the vapour phase to occupy a larger space of the tank. Removing vapour mass directly lowers the pressure of the tank since less vapour mass has the same space above the liquid to occupy. But due to the large difference in density between the vapour and liquid, seen in Figure 2-3, the same amount of extracted mass gives a large decrees in pressure when removing vapour mass and a small in comparison when removing liquid. Also due to the large density difference, the liquid mass occupy the vast majority of the tank, meaning that the actual temperature of the system is closely related to temperature of the liquid and as explained earlier, the actual tank pressure to the vapour space. This means that a fast reduction of the pressure due to removal of a large fraction of the vapour mass result in a new pressure-temperature equilibrium (a new liquid boiling point) according to 2-2 lower

than the one at the current liquid temperature. To reduce the liquid temperature to the new equilibrium (the new liquid boiling point temperature) at the new saturation pressure, the liquid phase need to travel down the liquid saturation line to the new equilibrium. It does so by rejecting its excess energy at the higher temperature state, by liquid evaporation, i.e. as L_v in equation 2.1. This of course again raises the pressure until the correspondence with the temperature is at equilibrium according to Figure 2-2.

2.2 Real cryogenic tank physics

The cryogenic temperatures of LNG makes the heat transfer mechanisms inside cryogenic tank complex. However it is shown in the thesis that satisfying modeling results can be obtained by using only a one dimensional linear heat transfer model. Although not incorporated in the modeling work presented in this thesis, the basics of the real heat transfer mechanisms for a cryogenic tank is described here. For completeness and as a base for future work.

2.2.1 Multilayer Insulation (MLI)

Cryogenic tanks often consist of one outer and inner shell with a vacuum drawn between them. These are often made of some austenitic stainless steel, due to its ability to withstand both impact and continuous load at cryogenic temperatures[13]. The outer shells purpose is to protect the tank against damage and hold the vacuum, since it is made out of steel it can be considered to have the same temperature as the ambient environment. The inner shell is covered with a Multilayer Insulation (MLI), which as the name suggest consist of layers of low conduction insulation materials combined with reflective, often metallic, materials [13] in multiple layers. Since no conduction or convection can occur in a perfect vacuum the heat transfer due to radiation will be the dominating heat transfer mechanism. It is because of this reason the shield materials are needed. In a real vacuum however gas conduction is also present[23] therefore the low conduction insulation material is needed to hinder the inevitable effects of conduction between the shielding layers. According to [23] the radiation heat transfer for a material with emissivity e and n reflective layers is reduced linearly with $e/(n+1)$ or e/n according to [13]. The heat transferred through the MLI is a complex combination of radiation, solid-contact conduction and gas conduction between layers[23]. A consequence of adding more layers is hence, increased contact points between layers and residual gas between layers. According to [14] the optimal layer density is between 45-55 cm^{-1} and it is also suggested that the thermal conductivity for MLI can be estimated between 2.6-5.5 W/mK.

2.2.2 Vapour cooling

For obvious reasons the inner shell of a cryogenic liquid tank must be connected to the outer shell. This creates a direct connection between the ambient temperated

outer shell and the cryogenic temperated inner shell. Also to be able to extract liquid from the tank piping must enter the liquid, creating a direct connection between the ambient temperated pipes and the cryogenic liquid. However, the heat flux through these paths to actually reach the liquid, can be greatly reduced by vapour cooling [13][23]. I.e. using the cold vapour to absorb the conducted heat through these components by a convective counter flow along the piping [13] and a continuous convection along the inner shell in contact with the vapour. The reduction of the shell temperature also reducing the radiative heat transfer reaching the liquid[23]. There is a one-to-one correspondence between the geometry and the vapour mass flow yielding zero conductance at the bottom of the pipe [13]. Meaning that if designed correctly the effect of conductance through piping in contact with the ambient environment could be completely eliminated. It also means that a pipe submerged into the liquid, will transfer different amounts of heat into the liquid bulk or non at all, dependant on the liquid level.

2.2.3 Inside of inner shell

It is well known that the major source of heat to enter the cryogenic liquid in the tank, is through the contact area between the liquid and the inner shell of the tank [13]. This heat flow together with vapour convection, radiation from warmer parts of the container e.t.c. aggregates to a small heat flow, typically around 100 W/m^2 entering the LNG [13]. These levels of heat flux are far to small for any nucleate boiling to occur, i.e. all mass transfer from liquid to vapour phase is due to surface evaporation which research shows [13]. The generally used term "boil-off" is hence misleading but will nevertheless be used in this thesis. The way the surface evaporation takes place is described in [13] and is summarised as follows: At the hot (higher temperature than the cryogenic liquid) vertical walls in contact with the liquid a high velocity convective current boundary layer is created, where heated liquid is transferred to the surface layers. At the surface the heated flow turns 90^o and then radially inward. During the transportation to the center of the liquid surface layer, evaporation from the super heated liquid takes place. Studies have shown the evaporation rate of this super heated flow to be almost linear to the degree of super heat of the liquid [13]. At the center of the surface layer the heated liquid flow is focused to a powerful downward jet, forcing the heated liquid into the liquid core. Where it releases its excess energy (the remainder not used for evaporation) to the liquid bulk and hence raising the total temperature of the liquid. The liquid at the bottom of the cryogenic container is heated and swept by the convection current to join the upward flow at the walls, thus completing the convection loop. The mass flow in the convection loop is measured many times greater than the total mass flow due to evaporation [13], suggesting that the majority of the heat flux entering the liquid is absorbed by this phenomenon.

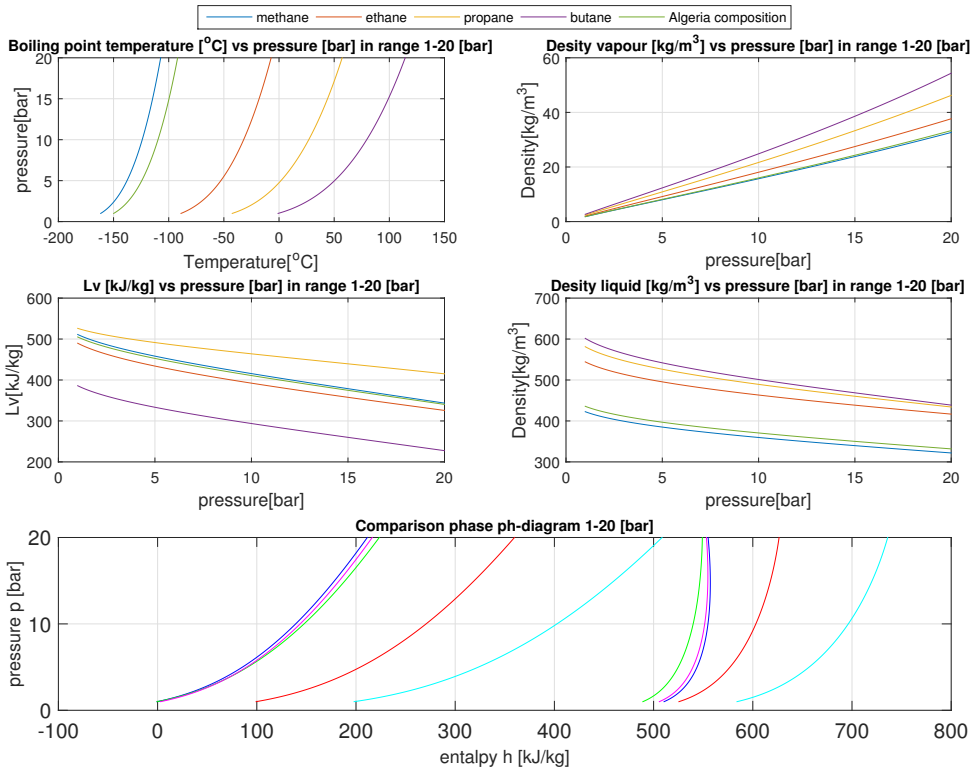

Figure 2-4: Comparison of saturation properties between the most common elements present in LNG. The mixture is a simple weighted mean of the components properties. The data is presented is in the pressure range relevant to a vehicular LNG tank. [3]

2.3 Assumptions

Due to the high fraction of methane in a typical LNG composition and the difficulties to determine the vapour quality in a real application as explained in 1.1.5, it is assumed in this thesis that the LNG consist of 100 % methane. This assumption is also a favorable base in an implementation so that if proven to be required, adaptation of the deviation from a 100 % methane model is possible. With this assumption no additional gas quality sensors or extra processing power is needed to determine NG quality, in agreement with the restrictions of the thesis to use a minimal amount of sensors. Furthermore under the assumption of a saturated system the saturation properties of a mixture does not diverge much from those of methane for the lowest composition in table 1.1 as seen in Figure 2-4. Note also that in the temperature range that will be experienced in the vehicular LNG tank (-162 to -110 explained in section 4.5 later on) the partial pressure of every component except for methane is close to zero [2], meaning that the vapour space will consist mainly of methane.

From section 2.1.2 it is assumed that a linear one dimensional heat transfer model can be used. This since the temperature gradient is stable due to the large temperature difference between the cryogenic and ambient environment. It is also a good

choice to avoid extra computational over head in an implemented model.

Furthermore it is assumed that the LNG tank is a saturated system, based on the discussion in section 2.1. Under these assumption the phase diagrams for a specific element is derived from empirical measurements [2]. Under the assumption of 100 % methane as LNG the saturation curve for methane can be used to determine the relation between states in an LNG tank. The empirical data can be obtained from for example [2]. This will be the base in this thesis for determining the tank system behaviour.

Chapter 3

System description

In this chapter the system that is to be modeled is described. The part numbers of the relevant system components appearing in the figures in this chapter is shortly explained in Table 3.1.

Table 3.1: Figure parts list.

Nr.	Component	Explanation
1	Check valves	Used prevent back flow from the tank when fueling and back flow through the fuel line.
2	Phase selector	Mechanical valve used to be able to draw both liquid and gas from the tank, explained in detail in section 3.3.2.
3	Manual valve	Used to close the fuel line manually.
4	Evaporator	Heat exchanger that evaporate the liquid to vapour and heat it.
5	Controlled valve	Solenoid valve controlled from an ECU, opened to enable NG flow between tank and engine.
6	Pressure relief valves	Used to vent NG from tank to prevent it from rupturing. One for normal use and one emergency.

3.1 Super insulated tank

The tank that is modeled in the thesis is a 529 liter LNG tank. It is constructed according to the explanation in section 2.2.1 and the combination of MLI and vacuum in such a construction is often referred to as super insulation. The usage of super insulation is general practise when designing cryogenic tanks [13] and is also suggested in [4] where a larger LNG tank than the one modeled in this thesis is modeled. Meaning that the heat transfer model from the ambient to the cryogenic environment, is applicable to most LNG tanks existing today.

3.2 Stationary operation

The reason for the usage of the super insulation in LNG containers are as mentioned in section 1.1.4 to enable the tank to be stationary when the vehicle is not used. The pressure relive solution in the system is two pressure relive valves as seen in Figure 3-1 and Table 3.1. The main relive valve is set to the maximum allowable working pressure (MAWP) of the tank, which is 16 bar for the modeled system. It's function is to maintain the pressure in the tank at the MAWP when the tank is left stationary for longer times. The alternate relive valve is an emergency valve set to 20 bar designed to open only if the main relive valve malfunctions. If the alternate relive valve has been opened once the tank should be removed from service and needs to be inspected.

3.3 Fuel delivery system

The way the LNG is extracted from and filled into the tank is described below. An illustration of the different fuel paths is shown in Figure 3-1.

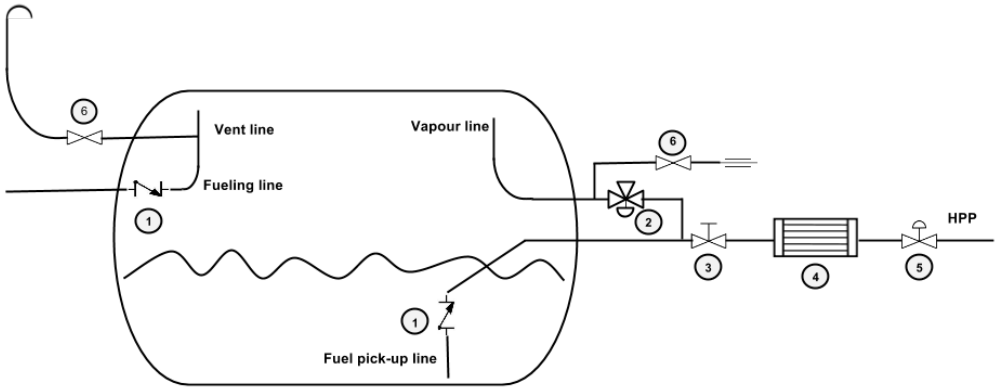

Figure 3-1: Principal schematic of the LNG tank modeled in the thesis.

3.3.1 Fueling of the tank

The modelled tank is filled by connecting the fueling station delivery hose to the fueling line seen in Figure 3-1. The tank pressure is first reduced to the desired pressure of the fueling station. The modelled tank is top filled i.e. when the fueling station starts delivering the sub cooled LNG through the fueling line in Figure 3-1, it is sprayed into the vapour space of the tank. By doing this the vapour in the tank condenses making room for the LNG eliminating the need to vent product due to a rising tank pressure, as would be the case in a bottom filled tank. This also means that the state of the tank after fueling will be that of the fueling station.

LNG is often transported on large ships, it is then stored in large containers in harbours (capacity around 160 000 m^3 [24]) with pressures around 1.05-1.3 bar [24].

It is then transported to the fueling station by a tanker truck, within the quite wide tank pressure range 1-8 bar [16]. Finally it arrives at the fueling station where it is delivered at the boil-off pressure accumulated in the supply chain. The highest tank pressure presented in [4], where a fueling station LNG tank is modeled, is 10.57.bar. The highest pressure one can expect is of course the fueling station vent pressure, if it does not exceed the MAWP. This all means that one can expect a vast variety in fuel station delivery pressures and hence vehicle fuel tank pressures after fueling, in a top filled tank. This also means that the theoretically lowest pressure one can expect from a fueling station is that of the large harbor containers. But due to boil-off during transport a more reasonable expected lowest is 3 bar [25]. Heavy vehicles might require higher tank pressures to be able to create any reasonable flow to the engine. Meaning that if the vehicle is fueled at this low pressure levels and a for example required tank pressure of 6 bar would be stuck at the fueling station for approximately 3 days according to the linearity in Table 5.1. Therefore a way to raise the tank pressure would be desirable, the model developed in the thesis could then be used for feed forward control of the tank pressure, in accordance with the purpose of the Master thesis in section 1.2.

In Figure 3-1 the pressure relive valves can be seen, they are both connected directly to the tank vapour space to ensure venting i all operation modes. The main relive valve is placed on the vent line to ensure the MAWP is not exceeded if the fueling station delivery pressure would exceed the MAWP in fueling operation. The alternate relive valve is placed on the vapour line to ensure a secondary evacuation path if the main relive valve vent line is malfunctioning and the MAWP is exceeded.

3.3.2 Fuel to engine

The liquid fuel delivery from the tank to the engine is driven by the pressure of the tank through the fuel line. However, the LNG tank is fitted with a so called Phase selector that allows vapour flow through the fuel line with the purpose to reduce the tank pressure to the Phase selector set point and by doing so cooling the system, as explained in section 2.1.3. The Phase selector, seen in Figure 3-1, is a mechanical valve which opens at its set point, 10 bar. When open, vapour will be delivered to the engine through the vapour line and when closed liquid will be delivered through the fuel pick-up line. The Phase selector is a non directional valve, allowing for back flow through the fuel line when the controlled valve is closed. Preventing liquid entrapment, which when evaporated could cause the fuel line piping to burst.

The Phase selector is assisted in its operation by an internal check valve providing a 0.14 bar back pressure in the fuel pick-up line. Creating a higher delivery pressure in the Vapour line during Phase selector operation, thereby ensuring pure NG delivery to the engine. This phenomenon will lead to different pressure drops in the fuel line dependant on whether vapour or liquid is delivered and needs to be addressed when placing pressure sensors in the fuel line.

3.3.3 Emptying the tank

When the liquid level in the tank is too low and the fuel pick-up line can't reach the liquid, vapour will flow through the fuel pick-up line rapidly reducing the tank pressure, as explained in section 2.1.3. This until the delivery pressure of the tank is not sufficient to create the required flow for the engine to function. This means that the lowest possible operating point of the tank system is this pressure, which for the modeled system is, 2.9 bar as seen later on in the measurement in Figure 5-5.

3.4 Current system sensors

Since no model over any system is ever completely correct, sensors are needed to correct an implemented model. The current LNG tank system only has a pressure sensor in the vapour delivery line, after the controlled valve seen in Figure 3-1, this location is referred to as the high pressure piping (HPP). It is also seen that this sensor is located after the heat exchanger, meaning that it does not have to be a cryogenic pressure sensor. I.e. the regulations on it is simpler and the cost of it is lower. The physical measurement of this sensor is also the tank pressure subtracted with the pressure drops over the components in the fuel delivery line. For experimental purposes an identical pressure sensor has been installed in the Vapour line in Figure 3-1. This measurement is naturally more stable than the one placed in the HPP since it does not experience the varying NG flows in the HPP due to varying engine load. The only other sensor that exist in the current system, relevant to a model of the process in the tank, is a tank level sensor integrated in the tank and calibrated by the tank manufacturer. It measures the capacitance of a capacitive tube inside the tank, which changes with the liquid volume fill of the tube. The calibrated sensor unit then outputs this as a measurable raw voltage.

Chapter 4

Modeling

In this Chapter the state space model is derived and presented. Two different implementation strategies are discussed and one is chosen for the vehicular LNG tank model developed in the thesis.

4.1 States and inputs

A state space model is chosen to describe the states of the LNG tank due to that many observer implementations require the model to be on this form and its practicality in implementation in general. The states chosen for the tank model state space system are

$$\bar{x} = \begin{pmatrix} T \\ p \\ V_l \\ m_g \\ m_l \end{pmatrix} \tag{4.1}$$

and are explained and derived in the following sub sections within this section. The inputs to the system are defined as

$$\bar{u} = \begin{pmatrix} T_{amb} \\ \dot{m}_{e,g} \\ \dot{m}_{e,l} \\ \dot{m}_v \end{pmatrix} \tag{4.2}$$

where the subscript e stands for engine and v for vent. The first inputs to the system are the ambient temperature in equation 2.7, T_{amb}. The other three mass flow inputs $\dot{m}_{e,g}$, $\dot{m}_{e,l}$ and $\dot{m}_{vent}$ are related to the mass extraction from the system and are covered below in section 4.3.

4.2 Energy balance

With the reasoning in section 2.1.1 and 2.1.2 gives that the energy balance over the whole system is

$$\dot{Q}_{in} = \dot{Q}_{heat} + \dot{Q}_{phase}. \tag{4.3}$$

Substitution equations 2.7, 2.5 and 2.4 into 4.3 gives the expression for transfer of mass between the phases as

$$\dot{m}_{BOG} = \frac{C(T_{amb} - T) - (c_{p,g}m_g + c_{p,l}m_l)\dot{T}}{L_v(T)}. \tag{4.4}$$

4.3 Mass states

When the tank is in stationary operation it can be considered as a closed system. I.e. no mass is extracted or introduced to the system and the mass flow inputs in equation 4.2 are zero. Hence, the mass transfer inside the cryogenic tank system is only through vaporisation and condensation $\dot{m}_{BOG}$. When the boil-off valve is opened a vapour mass flow $\dot{m}_v$ is extracted from the system. During vehicle operation either a liquid $\dot{m}_{e,l}$ or a vapor $\dot{m}_{e,g}$ mass flow is fed to the engine from the tank, due to the Phase selector . Since the model is intended for implementation the mass added to the tank when fueling it is not incorporated in the dynamical modeling since it is not guaranteed that the ECU, running the model, is powered up when fueling. Also since the tank after fueling will have the same state as the fueling station as described in section 3.3.1. It is better to reinitialize the model based on measurements after fueling. Hence the dynamic equations for the liquid and vapour mass flow are

$$\dot{m}_g = \dot{m}_{BOG} - \dot{m}_{e,g} - \dot{m}_v \tag{4.5}$$

$$\dot{m}_l = -\dot{m}_{BOG} - \dot{m}_{e,l}. \tag{4.6}$$

Substituting equation 4.4 and 2.6 into 4.5 and 4.6 give the mass state space equations with the correct states and input

$$\dot{m}_g = \frac{C(T_{amb} - T) - R\dot{T}}{L_v(T)} - \dot{m}_{e,g} - \dot{m}_v \tag{4.7}$$

$$\dot{m}_l = \frac{R\dot{T} - C(T_{amb} - T)}{L_v(T)} - \dot{m}_{e,l}. \tag{4.8}$$

4.4 Description of saturation properties

Under the assumptions of the thesis the relation between the states can be derived from the saturation properties of methane as described in section 2.3, i.e. the relations seen in Figures 4-1, 4-2, 4-3 and 4-4. Now, since this data is empirical, the accuracy of these relations are those of the empirical measurement from [2]. However, this

data will in the scope of the thesis be treated as the correct reference and all errors specified in this chapter are the deviation from the measured empirical data.

4.4.1 Relation between states

In Figures 4-1, 4-2, 4-3 and 4-4 the following relations can be seen

$$p = f_1(\rho_g), \tag{4.9}$$

$$T = f_2(p), \tag{4.10}$$

$$L_v = f_3(T), \tag{4.11}$$

$$\rho_l = f_4(T). \tag{4.12}$$

Where ρ_g and ρ_l is the vapour and liquid density respectively. The function f_i in equations 4.9, 4.10, 4.11 and 4.12, could be implemented as a look up table or an analytic function, describing the empirical saturation properties data from [2]. With different accuracy and computational time. The relations between states are chosen due to their linear or close to linear behaviour in the model pressure range to be used, described in section 4.5.

4.4.2 Description with look up tables

When f_i in equations 4.9, 4.10, 4.11 and 4.12 are implemented as look up tables the number of data points in the data maps is directly related to the accuracy and the calculation speed. I.e. more data points leads to less interpolation between data points and higher accuracy. But more iterations to extract the data from the arrays it is stored in. This is no problem on a computer but when used on an embedded system, with far less computing power it can be a problem. Large data maps also requires large storage space on the RAM for any reasonable computing time. This is also a problem on embedded systems where the RAM is limited. With the reasoning from section 1.1.6 it is important not to use large amounts of RAM and processing power for a single application.

4.4.3 Description with analytic functions

If instead an analytic function to describe the empirical data, is used, the need to store large amounts of data on the RAM and the need to perform the look-up operation on the array is eliminated. It is replaced with the calculation of the analytic function in each time step in the discrete time state space system. The CPU instructions required to calculate each analytic function in equations 4.9, 4.10, 4.11 and 4.12, depends on the order of f_i. I.e. a higher order equals more CPU instructions and hence longer computation time. The only data that needs to be stored on the RAM when using the analytic approach is the coefficients of the analytic functions f_i, which also increase with order. A downside is that the coefficients in the analytic function descriptions need to be re derived, off line, for other compositions of LNG, whereas with the

look up table implementation the data maps stored on the ECU can be adapted to fit the new composition of the LNG. The analytic approach is the one used in the model developed in the thesis, the analytic function descriptions f_i are polynomial descriptions of different order, derived with the least square method in MATLAB [3] with the function polyfit.

4.5 Model pressure range (2-16 bar)

Since the lowest operating point when emptying the tank is 2.9 bar as explained in 3.3.3 and that it is not reasonable to expect pressures lower than 3 bar following the reasoning in 3.3.1, the lowest operating point of the model is chosen to 2 bar. One could argue to choose 1 bar as the lowest point to cover the whole range from atmospheric pressure, but for some of the relations f_i in equations 4.9-4.12, the non-linearity in the 1-2 bar range lead to higher order polynomials required to be used as f_i. I.e. a simpler and therefore less computationally heavy model can be obtained by limiting the polynomial description to this range. The highest operating point chosen is 16 bar, in accordance with the discussion in section 3.2. Although chosen to this in the thesis, if the pressures above 16 bar is to be estimated with better accuracy, for example for diagnostic purposes the analytic functions f_i need to be modified to include the pressure range up to 20 bar, increasing the order and hence the computation time. To extend the pressure range above the secondary relive valve up to the critical pressure of 45.992 bar [2]. The Benedict-Webb-Rubin (BWR) Equation of state (EOS) [26] can be used [4][24], however this is a 6:th order exponential function description of the form $p = f(\rho_g, T)$ and hence require massive calculations only for f_1 in equation 4.9. Due to the modeling being implementation oriented, the BWR EOS can not be used for the model developed in the thesis.

4.6 Temperature state

The one-to-one correspondence between pressure and temperature for a saturated system seen in Figure 2-2 and can be used to describe the relation between the pressure and temperature in a saturated system as explained in section 2.1. To get as short as possible computational times as described in section 4.4 in the range specified in 4.5. A third order polynomial function is used for the description of the empirical data of the saturation properties obtained from [2]. The third order is needed for an acceptable accuracy, due to the non linear relation between the pressure and temperature in the modeling pressure range. The function f_2 in equation 4.10 hence becomes

$$T = a_p p^3 + b_p p^2 + c_p p + d_p, \tag{4.13}$$

where the coefficients can be found in Table 4.1. The function in equation 4.13 can be seen in Figure 4-1 and the errors are found in Table 4.1. Time differentiating equation 4.13 yields

$$\dot{T} = (3a_p p^2 + 2b_p p + c_p)\dot{p} = k_p \dot{p}, \tag{4.14}$$

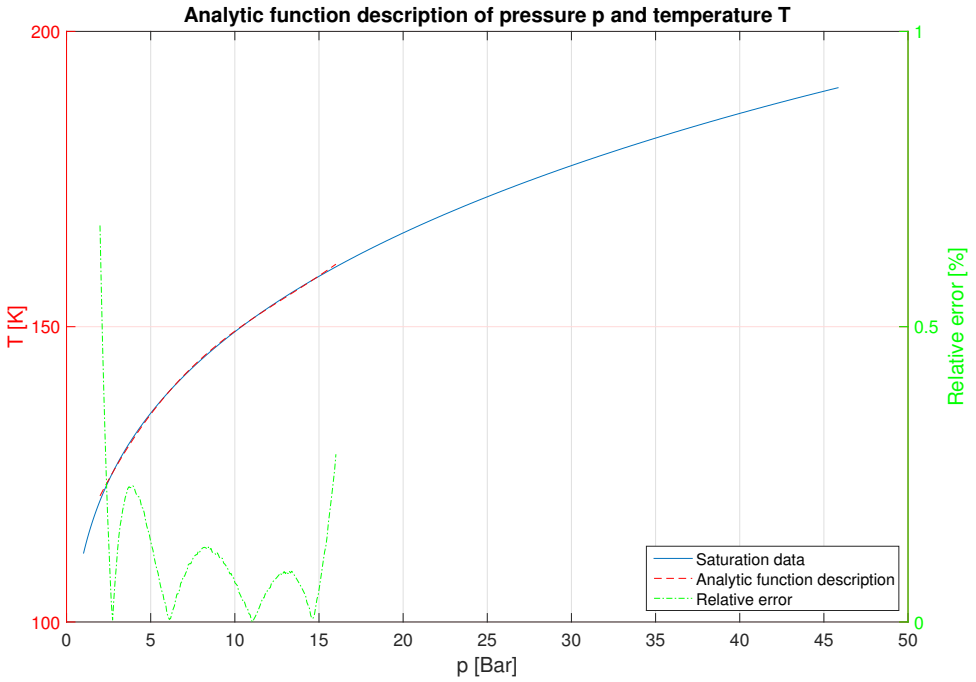

Figure 4-1: Third order analytic function description $f_2(p) = a_p p^3 + b_p p^2 + c_p p + d_p$ compared to the data from [2]. [3]

Which is the state equation for the temperature. Note that k_p in equation 4.14 can be any analytic expression differentiated with respect to p according to the chain rule if higher or lower accuracy is desired. It can also be changed to some numeric derivative of the data map with desired step length, for example central difference, Euler backward or forward, when using the look up table implementation approach.

4.7 Basic equations

The physical volume of the tank is defined constant as V and the liquid volume as the state V_l. The vapour volume is hence

$$V_g = V - V_l. \tag{4.15}$$

The volume of the modeled tank described in Chapter 3 is

$$V = 0.529m^3 \tag{4.16}$$

and the time derivative of equation 4.15 is

$$\dot{V}_g = -\dot{V}_l. \tag{4.17}$$

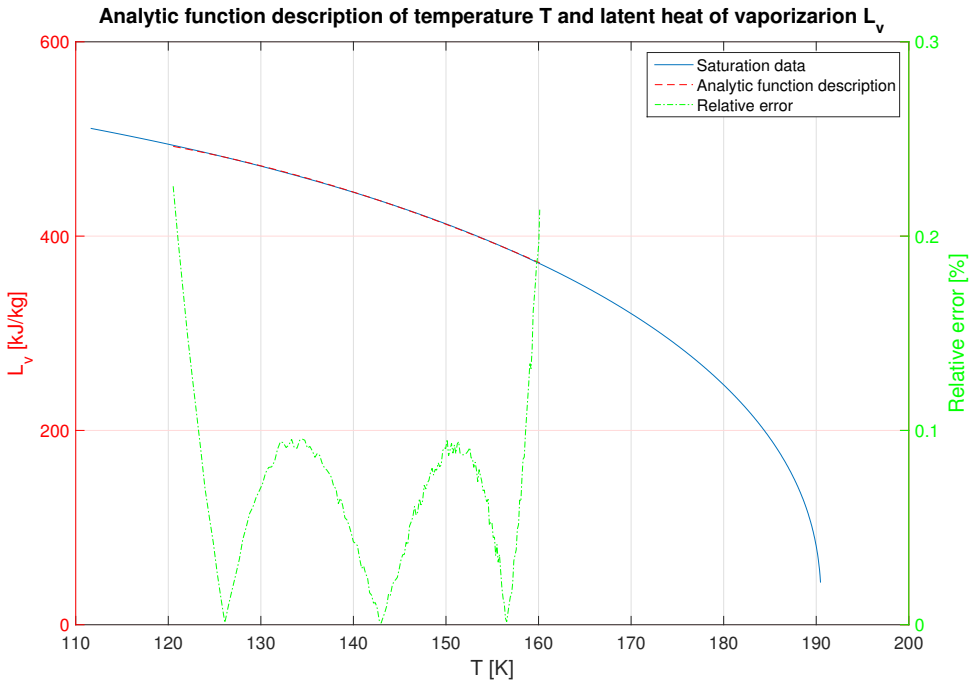

Figure 4-2: Second order analytic function description $f_3(T) = a_{L_v}T^2 + b_{L_v}T + c_{L_v}$ compared to the data from [2].[3]

The relation between mass m_x, volume V_x and density ρ_x for both liquid and vapour is the well known equation

$$\rho_x = \frac{m_x}{V_x} \tag{4.18}$$

and the time derivative is

$$\dot{\rho}_x = \frac{\dot{m}_x}{V_x} - \frac{m_x}{V_x^2}\dot{V}_x. \tag{4.19}$$

The mass state equations 4.7 and 4.8 depend on the latent heat of vaporisation $L_v(T)$, as a function of the saturation temperature. Therefore a analytic function description as f_3 of the relationship in equation 4.11 is required. Due to the light non-linear behaviour of the empirical data of $L_v(T)$ in the model pressure range described in section 4.5 the second order polynomial

$$L_v = a_{L_v}T^2 + b_{L_v}T + c_{L_v} \tag{4.20}$$

is used to described the empirical data, as seen in Figure 4-2. The coefficients of 4.20 and the deviation from the empirical data is given in table 4.1.

4.8 Liquid volume state

Due to the empirical data for the relation in equation 4.12, having a linear behaviour in the pressure range motivated in section 4.5, as seen in Figure 2-3. A linear function

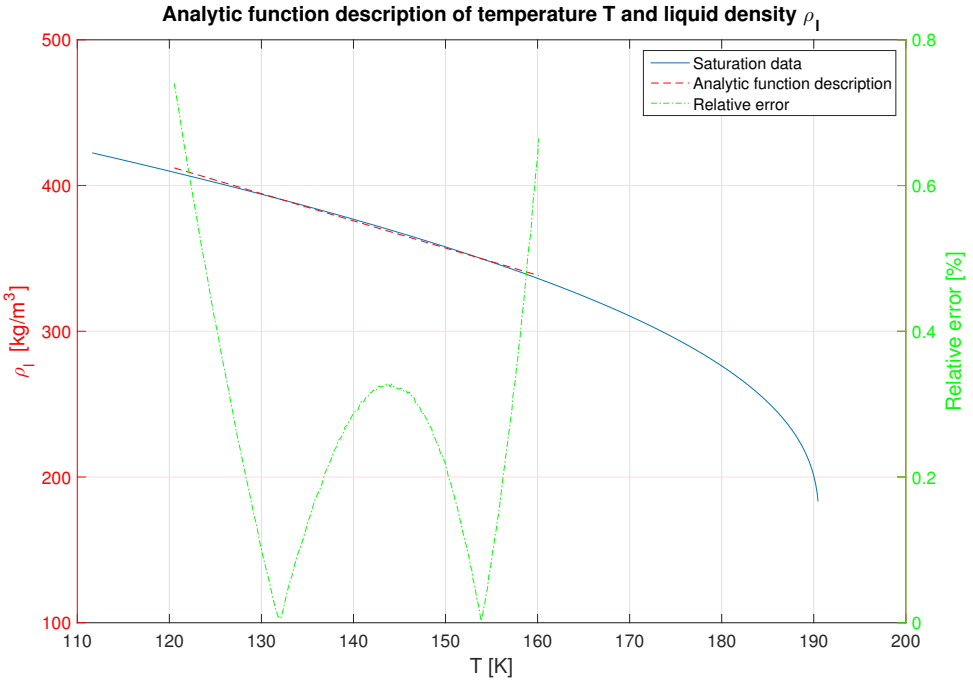

Figure 4-3: Linear analytic function description $f_4(T) = a_T T + b_T$ compared to the data from [2].[3]

for f_4 is chosen for the model developed in the thesis,

$$\rho_l = a_T T + b_T, \tag{4.21}$$

The analytic function between the liquid density ρ_l and the temperature T can be seen in Figure 4-3. the coefficients in equation 4.21 and the deviation from the empirical data can be found in Table 4.1. By time differentiating equation 4.21,

$$\dot{\rho}_l = a_T \dot{T} \tag{4.22}$$

is obtained. Note once again that a_T can be any analytic expression or numerical approximation, differentiated with respect to T. Inserting equation 4.22 into equation 4.19 and solving for $\dot{V}_l$, gives the liquid volume state equation

$$\dot{V}_l = \frac{\dot{m}_l}{m_l} V_l - a_T \frac{V_l^2}{m_l} \dot{T}. \tag{4.23}$$

4.9 Pressure state

In the pressure range described in section 4.5 the relation in equation 4.9 is also quite linear as seen in Figure 4-4. Therefor a linear analytic function is selected for the state equation of the tank pressure p, to keep the computational time as short as

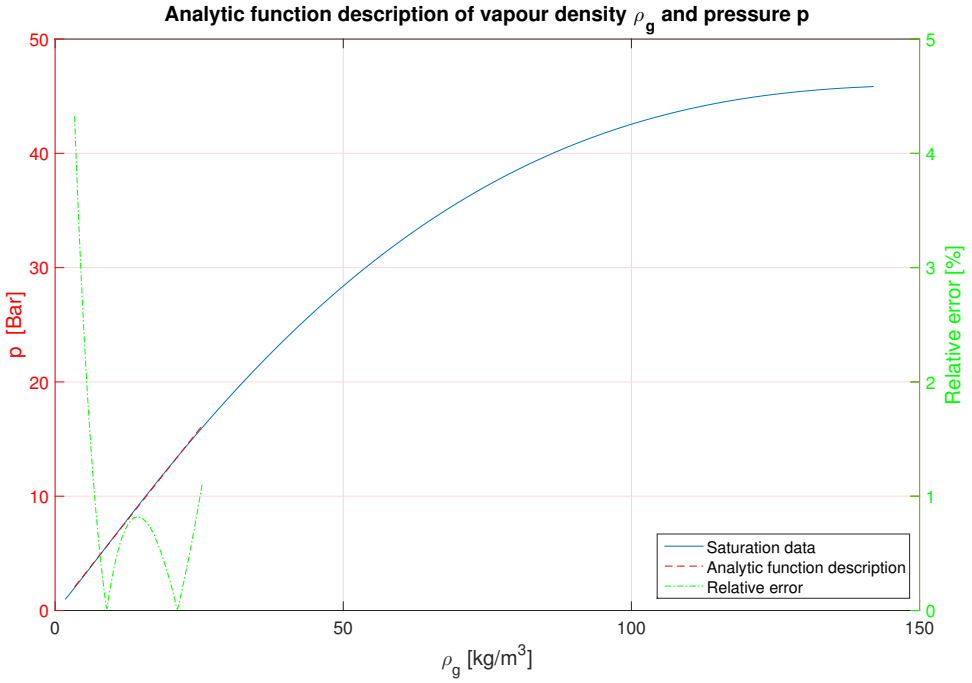

Figure 4-4: Linear analytic function description $f_1(\rho_g) = a_\rho \rho_g + b_\rho$ compared to the data from [2].[3]

possible. Equation 4.9 then becomes

$$p = a_\rho \rho_g + b_\rho, \tag{4.24}$$

The linear analytic function description of the empirical data for the relation between pressure and vapour density is seen in Figure 4-4 and the coefficients of equation 4.24 and the error of the function description can be fond in table 4.1. Time differentiating equation 4.24 gives

$$\dot{p} = a_\rho \dot{\rho}_g. \tag{4.25}$$

Note again the form of equation 4.25, the constant a_ρ could be replaced with any higher order analytic expression differentiated with respect to ρ_g for a higher order description of the relation in equation 4.9. Inserting equation 4.19 in 4.25 and making use of equation 4.15 and 4.17, for the correct states yields

$$\dot{p} = a_\rho \frac{\dot{m}_g}{V - V_l} + a_\rho \frac{m_g}{(V - V_l)^2} \dot{V}_l. \tag{4.26}$$

Inserting the state equations for T, V_l, m_g and m_l, 4.14, 4.23, 4.7 and 4.8 into 4.26, combined with equations 2.7, 2.6 and solving for $\dot{p}$ gives the final state equation for the pressure

$$\dot{p} = a_\rho \frac{m_l \dot{Q}_{in}(V - V_l) - m_l(V - V_l)L_v(\dot{m}_{e,g} + \dot{m}_v) - m_g V_l \dot{Q}_{in} - m_g V_l L_v \dot{m}_{e,l}}{m_l L_v (V - V_l)^2 + a_\rho R k_p m_l (V - V_l) - a_\rho R k_p m_g V_l + a_\rho a_T k_p m_g L_v V_l^2}. \tag{4.27}$$

Table 4.1: Coefficients and the relative percentage error of the analytic function descriptions of the the data maps obtained from [2] for saturated methane.

Equation	Order	Coefficients	Mean [%]	Max [%]	Boundary (2bar,16bar)[%]
4.24	1	$a_\rho = 63699.68171328756$ $b_\rho = -7761.152686900214$	0.8475	4.3255	(4.3255,1.1099)
4.13	3	$a_p = 9.8 \cdot 10^{-18}$ $b_p = -3.88 \cdot 10^{-11}$ $c_p = 6.92 \cdot 10^{-5}$ $d_p = 109.039788$	0.1050	0.6714	(0.674,0.0.2840)
4.20	2	$a_{L_v} = -30.406815022776930$ $b_{L_v} = 5505.735479337756$ $c_{L_v} = 270510.4370240070$	0.0684	0.2257	(0.2257,0.2136)
4.21	1	$a_T = -1.865525108868322$ $b_T = 636.9605750739277$	0.2571	0.7404	(0.7404,0.6649)

4.10 Discrete time

To get the non-linear state space on discrete time form an Euler forward is used with sample time T_s, chosen as high as possible to use as little resources as possible, but small enough to maintain acceptable accuracy. The state equations will not be written explicitly, but with dependence on each other to save space and since they can be implemented in this way. With this and rewriting equation 4.27 the discrete time state space equations then follows as:

$$p_{[n+1]} = \Psi_{[n]} = p_{[n]} + T_s dp_{[n]} = p_{[n]} + \frac{T_s a_\rho (m_{l[n]}(V - V_{l[n]})(\dot{Q}_{in[n]} - L_{v[n]}(\dot{m}_{e,g[n]} + \dot{m}_{v[n]})) - m_{g[n]} V_{l[n]}(\dot{Q}_{in[n]} + L_{v[n]}\dot{m}_{e,l[n]}))}{m_{l[n]}(V - V_{l[n]})(L_{v[n]}(V - V_{l[n]}) + a_\rho R_{[n]} k_{p[n]}) + a_\rho k_{p[n]} m_{g[n]} V_{l[n]}(a_T L_{v[n]} V_{l[n]} - R_{[n]})} \tag{4.28}$$

$$T_{[n+1]} = \Upsilon_{[n]} = T_{[n]} + T_s k_{p[n]} \Psi_{[n]} \tag{4.29}$$

$$V_{l[n+1]} = V_{l[n]} + T_s \left(\frac{\Phi_{[n]}}{m_{l[n]}} V_{l[n]} - \frac{V_{l[n]}^2}{m_{l[n]}} a_T \Upsilon_{[n]} \right) \tag{4.30}$$

$$m_{g[n+1]} = m_{g[n]} + T_s \left(\frac{\dot{Q}_{in[n]} - R_{[n]} \Upsilon_{[n]}}{L_{v[n]}} - \dot{m}_{e,g[n]} - \dot{m}_{v[n]} \right) \tag{4.31}$$

$$m_{l[n+1]} = \Phi_{[n]} = m_{l[n]} + T_s\left(\frac{R_{[n]}\Upsilon_{[n]} - \dot{Q}_{in[n]}}{L_{v[n]}} - \dot{m}_{e,l[n]}\right) \tag{4.32}$$

Where the subscript n is defined as the current time step.

Chapter 5

Evaluation and implementation

In this Chapter other research in the field of modeling cryogenic LNG containers is discussed and its validity in a vehicular application is evaluated. The computer implementation of the LNG vehicular tank model developed in the thesis is presented and a prof of concept Extended Kalman filter (EKF) as a model observer is suggested and evaluated. The simulation results of the developed model and the EKF is also presented.

5.1 State of the art

In this section related research in the field of cryogenic tank modeling is discussed.

5.1.1 Similar systems

Due to that the LNG vehicular market is still small as described in section 1.1.3 there exist virtually no research on LNG tanks in vehicular application. And the one that do are either concerned with mechanical design of an LNG tank [27] or engine emissions for different compositions of NG [18]. The research closest in relation to the thesis is [4] where a fueling station tank of 56.781 m^3 and 49.211 m^3 capacity is modeled during stationary operation. The model proposed in [4], section "3. Dynamic process during LNG storage and fueling" is quite similar to the model proposed in this thesis (in section 5.4.2), since both a linear heat transfer model is used and the heating of the cryogenic liquid and vapor is taken into account. The major difference besides the obvious fact that the input to the system in [4] are those of a fueling station LNG tank, is that [4] is using the BWR EOS [26] to determine the tank pressure instead of the saturation properties of methane as proposed in the thesis. Despite this the similarity of models enables the simulations done in [4] to be preformed with the model presented in section 5.4.2 and compared for the purpose of benchmarking the model developed in the thesis, with real measured data during static operation available in [4].

A way of determining the super heat transfer coefficient C in equation 2.7 is

suggested in [4] based on the geometry, heat conductance and thickness of the MLI and steel of the inner shell of the tank. The equation for C in [4] is not used in the thesis since the exact geometry and the MLI thickness of the modeled tank could not be obtained from the tank manufacturer. Instead C is estimated from the measurements presented in section 5.3.1. It is however, based on the results of [4], recommended for future work to use the procedure for determination of C in [4] for a model implemented on an ECU for calibration simplification. If the required parameters are known and the calculated value corresponds well with the estimated value in section 5.4.2.

5.1.2 Large LNG containers

Most research on modeling of the process inside an LNG tank is concerned with the boil-off in large LNG containers with capacity's in the range of 160 000 m^3 [24]. In these large tanks the pressure is kept around atmospheric i.e. temperatures around -160 ^oC [24]. I.e. a smaller scale tank like a vehicular tank has a much wider pressure range that it operates in. Therefore the boil-off model with constant heat of vaporisation in equation 5.1 is not suitable for small scale tank modeling.

$$\dot{m}_{BOG} = \frac{\dot{Q}_{in}}{L_v}[4][28][24]. \tag{5.1}$$

In [24] the boil off rate is modeled with equation 5.1 and the states of the LNG in different large containers is modeled with two different models. A model based on the Lee-Kesler-Plocker (LKP) equation which is based on the general compressibility ideal gas law [22] and the BWR EOS. The LKP equation, like the BWR EOS, is exponential and of 6:th order, making also the LKP equation highly inappropriate for implementation on an embedded system. [24] makes the assumption that the density and temperature of the LNG is constant in the tank which is not a valid assumption in a large pressure range (section 4.5) needed for a model over a vehicular tank. It is hence concluded that the way of modeling or the results from [24] can not be used in the thesis.

A more extensive non-linear heat transfer model than the one used in this thesis is used in [28]. But in [28] the thermal stress in a large capacity LNG tank is considered and since it is the process in the tank that is the main concern of this thesis. The heat transfer trough individual parts of the tank is not considered and the linear heat transfer model in equation 2.7 is used. In [28] the simplified boil-off model 5.1 is also used.

5.1.3 Extended Kalman filter (EKF) and LNG

Since there exist very little research on vehicular LNG tank modeling there exist even less research on Kalman filtering in the topic. However, there exist vast amounts of literature on the subject of Kalman and Extended Kalman filters and the way to

implement them is almost identical regardless of the system to be filtered. In [16] the dangerous states of a large vehicular transport tank is predicted through Multi-data sensor fusion. Among the methods used for this are Kalman filtering. The method used in [16] is not presented explicitly but the results are very satisfying. Due to the destructive power of a BLEVE from a malfunctioning LNG tank, it is a very good idea to incorporate such functionality in a vehicular fuel tank. With this in mind, a prof of concept EKF for the model developed in the thesis is presented in this Chapter in section 5.5.

5.2 Computer implementation

The model developed in the thesis is ultimately to be implemented on an embedded system. But in the scope of the thesis it is only implemented on a computer in simulink [3] for simulation and in MATLAB [3] for the extended Kalman filter. With consideration taken to that it should be implemented on an embedded system, the MATLAB code implementation of the model, used for the EKF, is translatable to C-code that can be run on an embedded system. But data type selection and some optimisation in computing time against accuracy should be performed when the model is implemented in an embedded system.

5.2.1 Initial values

The only initial values required to initialize the model is the initial tank pressure p_0 and the initial tank level $level_{tank0}$ in % defined as

$$level_{tank} = \frac{V_l}{V} \tag{5.2}$$

in accordance with the sensor measurement in section 3.4. These two states are needed to be able to determine all states of the tank since the pressure decides in what saturation state the tank is in (what temperature and pressure is present in the tank) and the tank level decides how big the vapour space of the tank is and hence how much of the LNG in the tank is vapour mass and how much is liquid mass. With the initial pressure set to p_0, the initial state T_0 can be computed with equation 4.13. With equation 5.2 and $level_{tank0}$ the initial state V_{l0} is obtained. With equations 4.18, 4.24, 4.15, p_0 and V_{l0}, the initial state m_{g0} is obtained. With equation 4.21, T_0 and V_{l0}, the initial state m_{l0} is obtained. Hence all the initial states is computed and the model initialized.

5.2.2 Phase selector implementation

While there are two inputs $\dot{m}_{e,g}$ and $\dot{m}_{e,l}$ in the discrete time state space equations 4.28, 4.29, 4.30, 4.31 and 4.32. The engine only consumes one mass flow $\dot{m}_e$ and a model implementation should keep track of if vapour or liquid is extracted from

the tank. In the physical system it is the Phase selector that makes this distinction, described in section 3.3.2. Therefore the Phase selector is simply implemented as

$$p \begin{cases} > 10 \text{ bar}, & \dot{m}_{e,g} = \dot{m}_e,\ \dot{m}_{e,l} = 0 \\ < 10 \text{ bar}, & \dot{m}_{e,g} = 0,\ \dot{m}_{e,l} = \dot{m}_e \end{cases} \tag{5.3}$$

I.e even though the input in the state space equations is dual, the input to the actual model application is only the engine consumption which requires more calculation for the ECU running the model application but is a more optimal solution in a distributed system since less data needs to be sent on the data bus. I.e. the only data transmission required by the model application implemented like this is the engine consumption $\dot{m}_e$ and the ambient temperature T_{amb} if the ECU running the application is not measuring these parameters.

5.2.3 Emptying tank implementation

The phenomenons described in section 3.3.3 when emptying the tank, is implemented in the model implementation as if the liquid volume is less than 10 l the fuel pick-up line can't reach the liquid and vapour is delivered trough it instead. The lowest possible delivery pressure is once again 2.9 bar. Combining these conditions and 5.3 gives the full conditions on $\dot{m}_{e,g}$ and $\dot{m}_{e,l}$

$$V_l \begin{cases} > 10\ l \text{ and } p > 10 \text{ bar}, & \dot{m}_{e,g} = \dot{m}_e,\ \dot{m}_{e,l} = 0 \\ > 10\ l \text{ and } 2.9 < p < 10 \text{ bar}, & \dot{m}_{e,g} = 0,\ \dot{m}_{e,l} = \dot{m}_e \\ < 10\ l \text{ and } 2.9 < p < 10 \text{ bar}, & \dot{m}_{e,g} = \dot{m}_e,\ \dot{m}_{e,l} = 0 \\ < 10\ l \text{ and } p < 2.9 \text{ bar}, & \dot{m}_{e,g} = 0,\ \dot{m}_{e,l} = 0 \end{cases} \tag{5.4}$$

Hence no consideration is taken in the implementation to the tilt of the tank. This is because it requires more input to the model making it more consume more resources, such as sensor or data transmission in a distributed system, to determine the angle of the vehicle at which the tank is mounted. Such an implementation also requires more dynamics in the model implementation making it more computationally heavy. Also as have been covered earlier since the construction of the inside of the tank is not known the dynamics will be hard to identify.

5.2.4 BOV implementation

The specifications of the BOV could not be obtained from the tank manufacturer so a very simple conditional flow model with a hysteresis of 0.1 bar has been used in the simulink model, and gives the vented mass flow $\dot{m}_v$ as

$$\dot{m}_v = \sqrt{\frac{2A(p,\dot{p})m_g(p - p_{atm})}{V - V_l}}.$$

With the conditions of the opening area of the valve as

$$A(p,\dot{p}) = \begin{cases} A_s, & \text{if } p > 16 \text{ bar and } \dot{p} > 0 \\ A_s, & \text{if } p > 15.9 \text{ bar and } \dot{p} < 0 \\ 0, & \text{else} \end{cases}$$

Where A_s is the opening area times a flow constant set to 10^{-11} to be able to cope with longer sample times. The BOV is only implemented in the simulink model for simulation purposes since it is not intended for it to be opened during vehicle operation, when a ECU running the model would be powered up. I.e. during model execution in a real application $\dot{m}_v$ should be set to zero in the state equations 4.27, 4.14, 4.23, 4.7, 4.8, 4.28, 4.29, 4.30, 4.31, 4.32. Furthermore, the Phase selector and the fact that the tank is top filled makes the opening of the BOV highly unlikely. Therefore it is not recommended to implement any model of the BOV in a system similar to the one modeled in this thesis, since it only creates unnecessary overhead for the ECU hosting the model application. It might however be suitable to implement a more accurate model for the BOV in the simulink model intended for simulation purposes, since it could for example be interesting to simulate how much product is lost when the tank is stationary for very long periods.

5.2.5 Saturation

The liquid volume state is saturated between the modeled LNG tanks maximum capacity, equation 4.16, and 1 l since a volume can't be negative and to prevent the pressure singularity at 0 liquid volume and hence 0 liquid mass seen in equation 4.28. This is because the model is a two-phase model and for the situation when there is no liquid in the tank, an other model is required, for example the ideal gas law [22]. The mass states are saturated at 1 g as the lowest possible mass also to avoid the pressure singularity when there is 0 mass in the tank, seen in equation 4.28.

5.3 Verification data

Two testes has been carried out on a Scania NGV during vehicle operation. One when emptying the LNG tank at low loads and one at full load. Indicative hold time data is provided by the tank manufacture [6] and the model developed in the thesis is compared to the hold time data presented in [4].

5.3.1 Measured data light load

The data presented in this section is from a run with a Scania NG truck which is unloaded, until the tank is considered empty. The available and needed input to the model is the engine consumption $\dot{m}_e$ which is measured in the vehicle and seen in Figure 5-1. The output from this run available for comparison is the pressure in the LNG tank p, also in Figure 5-1. The liquid level sensor was not calibrated at this

measurement so the initial tank level was estimated to $level_{tank0} = 46$ % by simulation of the model developed in the thesis, so that the tank model is empty when the real tank in the measurement is empty. The output from the liquid level sensor is a voltage and that has been linearly calibrated between $level_{tank0} = 46$ % and $level_{tank0} = 0$ % for the maximum and minimum voltage data. This is to be able to use it in the model implementation. The raw measurement voltage and the calibrated result is seen in Figure 5-2. Also in this measurement the pressure sensor placed in the HPP is available, in Figure 5-2, to be used in the extended Kalman filter application as will be shown later on. Note that the pressure measurements at light load are in gauge i.e. relative to atmosphere.

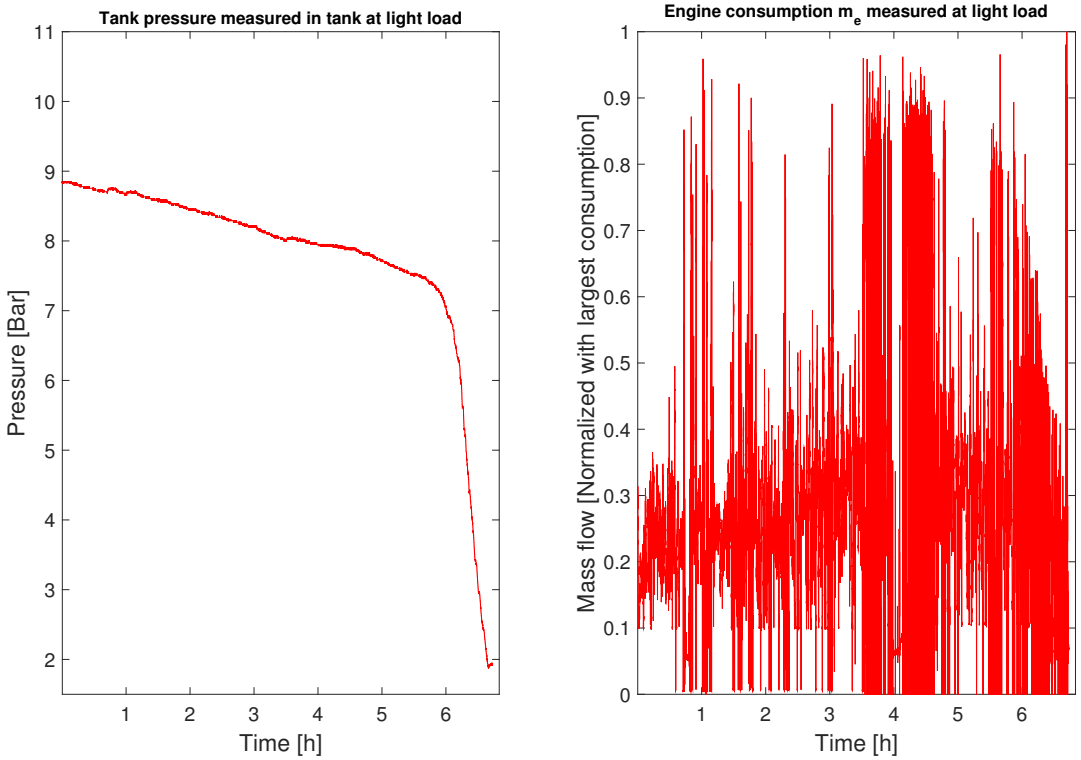

Figure 5-1: Tank pressure sensor and engine consumption measurement for light load of a NG truck [3].

5.3.2 Measured data Full load

The data presented in this section is from a run with a NG truck which is loaded with approximately 17 tons, until the tank is considered empty. The available input from this measurement is both the ambient temperature T_{amb} and the engine consumption $\dot{m}_e$ seen in Figure 5-3. From this measurement also the temperature of LNG T is available, measured on the fuel line piping exiting the tank. Again the LNG tank pressure p measured in the tank is available. The comparison data available is seen in Figure 5-4. The liquid level sensor was not available during this measurement so

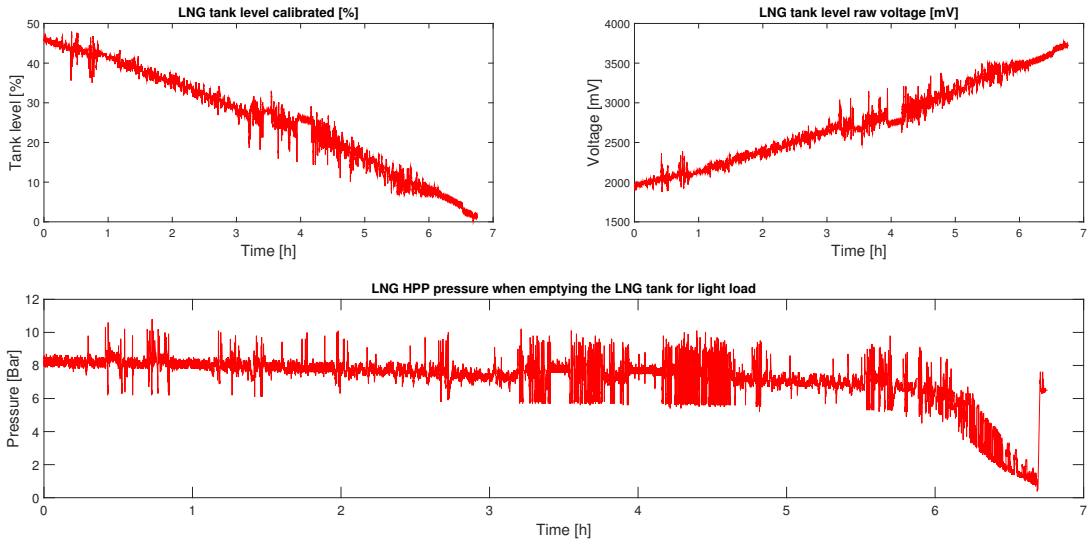

Figure 5-2: HPP pressure sensor and liquid level sensor measurement for light load of a NG truck [3].

the initial tank level was estimated to $level_{tank0} = 60$ % again by simulation of the developed model so the real and modeled tank are emptied at the same time.

5.3.3 Indicative stationary data from tank manufacturer

The available data for verification of the tanks hold time during stationary operation is limited and only indicative, therefore the conclusions drawn from this data is not definite. The tank manufacturer specify that with their super insulation the tank will have a hold time of over a week [6]. However no tank size, tank fill level or initial pressure is specified for this. I.e. no initial state is possible to determine from this, but it gives an indication in what range the hold time should be. Furthermore an indicative table of hold times for full tank fill level and different initial pressures are provided by the tank manufacturer, seen in Table 5.1. Provided as an indication to the customer how long he/she can park the vehicle inside without venting LNG. With this in mind, most likely, the hold times have been rounded down to be on the safe side so that flammable gas is not vented if the vehicle is parked inside. With a hold time of 5 days between 10-16 bar according to Table 5.1, full tank 165.5 kg in the 10-16 bar range, one realize by looking in Figure 2-1 that this represent around 19 W of heat flow $\dot{Q}_{in}$ into the tank.

5.3.4 Data from Q.s. Chen et al.

Like mentioned in section 5.1.1, [4] provides measurement data from a Beijing 56.781 m^3 (15,000 gallon) LNG fueling station tank, that is stationary for 5 days. The initial pressure in the measurement is 9.67 bar (140.2 psi) and the pressure after 5 days is 10.57 bar (153.3 psi). The initial fill of the tank is 9.7323 m^3 (2571 gallons), i.e. a $level_{tank}$ of 17.2 %. The model developed in [4] have the same heat transfer model as

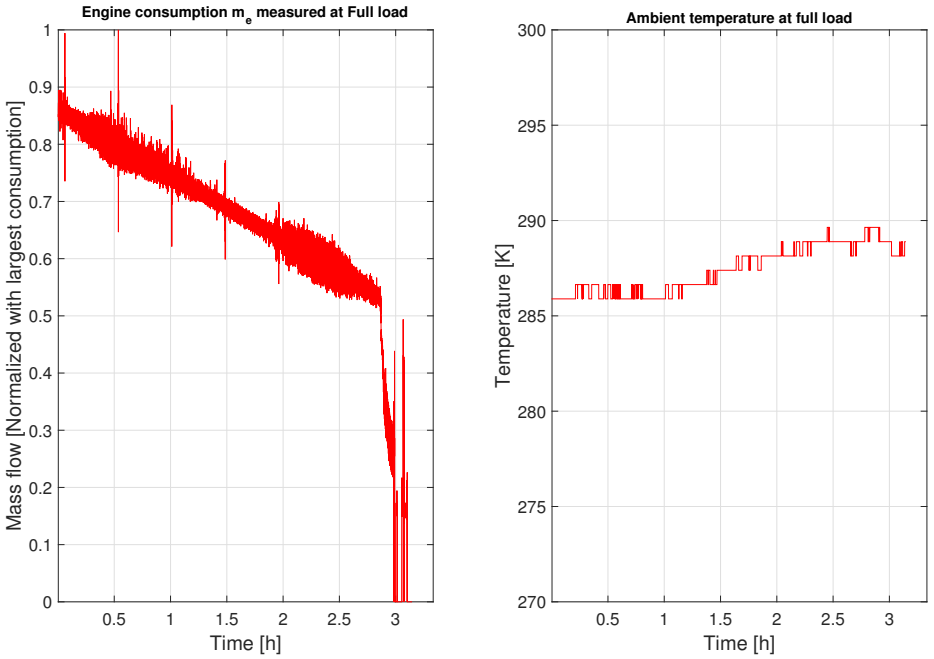

Figure 5-3: Engine consumption normalized with the largest consumption and ambient temperature measured at full load of a NG truck, to be used as input to the model for verification [3].

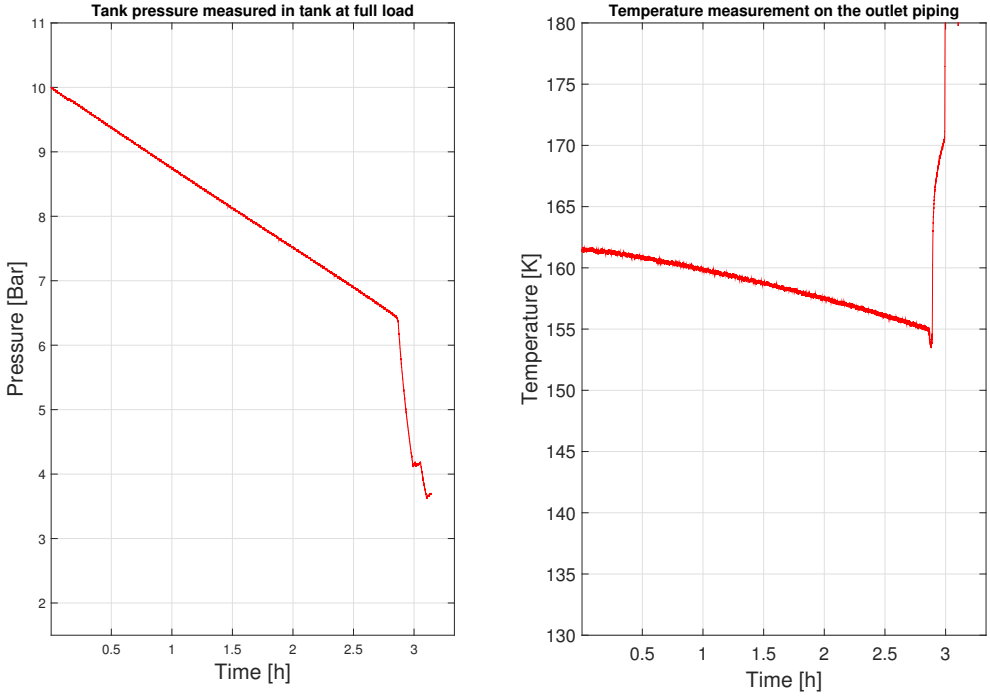

Figure 5-4: Tank pressure and temperature measured at full load of a NG truck, to be compared to the model for verification [3].

Table 5.1: Indicative Hold times for different initial tank pressures for a full LNG tank [6]

Tank pressure	Hold time
10 bar	5 days.
11 bar	4 days
12 bar	3 days
13 bar	2 days
14 bar	1 day

in this thesis in equation 2.7. The heat transfer coefficient C is estimated to 1 W/K in [4]. The final saturation pressure for the model simulation performed by Q.s. Chen et al. in [4] was 10.71 bar (155.27 psi) which corresponds well with the measured data from the fueling station.

5.4 Evaluation and Verification of models

Two different ways to model the system has been investigated in the thesis and are presented in this section. In all simulations in this section the ambient temperature is set to 20 ^{o}C, when not specified otherwise, since due to the large temperature difference between the cryogenic LNG and normal ambient temperatures a variation in T_{amb} does not affect the result considerably. A sample time T_s of 10 s is used for all simulations to show the model robustness and exactness in this incredibly long sample time. Like in most cases better accuracy is achieved with a lower T_s, however it will be seen in this section that the results presented with $T_s = 10$ s are satisfying.

5.4.1 Simplified BOG model

Like mentioned in section 5.1 most modeling of the states in the LNG tank only considers the boil-off as the mechanism that raises the pressure of the tank. I.e. the energy balance in equation 4.3 with equation 5.1 transforms to

$$\dot{Q}_{in} = \dot{Q}_{phase} \tag{5.5}$$

since, now $\dot{Q}_{heat} = 0$. Physically this means that all of the heat flow that enters the tank is absorbed by the cryogenic liquid and is used for evaporation directly. I.e. the heating of liquid and vapour discussed in section 2.1.1 is neglected, which means that a big part of the cryogenic system's resistance to heat is not considered. The major difference between these two types of modeling is hence the time to the opening of the BOV in stationary operation. I.e for the same heat flux $\dot{Q}_{in}$ from equation 2.7, this way of modeling will give a shorter boil-off valve opening time (BOVOT) since it has lower heat resistance. With the assumption in equation 5.5 the state space

equations 4.28, 4.29, 4.30, 4.31 and 4.32 simplify to

$$p_{[n+1]} = p_{[n]} + \frac{T_s a_\rho (m_{l[n]}(V - V_{l[n]})(\dot{Q}_{in[n]} - L_{v[n]}(\dot{m}_{e,g[n]} + \dot{m}_{v[n]})) - m_{g[n]} V_{l[n]}(\dot{Q}_{in[n]} + L_{v[n]}\dot{m}_{e,l[n]}))}{m_{l[n]} L_{v[n]}(V - V_{l[n]})^2 + a_\rho a_T k_{p[n]} L_{v[n]} m_{g[n]} V_{l[n]}^2} \tag{5.6}$$

$$T_{[n+1]} = T_{[n]} + T_s k_{p[n]} p_{[n+1]} \tag{5.7}$$

$$V_{l[n+1]} = V_{l[n]} + T_s \left(\frac{m_{l[n+1]}}{m_{l[n]}} V_{l[n]} - \frac{V_{l[n]}^2}{m_{l[n]}} a_T T_{[n+1]} \right) \tag{5.8}$$

$$m_{g[n+1]} = m_{g[n]} + T_s \left(\frac{\dot{Q}_{in[n]}}{L_{v[n]}} - \dot{m}_{e,g[n]} - \dot{m}_{v[n]} \right) \tag{5.9}$$

$$m_{l[n+1]} = m_{l[n]} + T_s \left(\frac{-\dot{Q}_{in[n]}}{L_{v[n]}} - \dot{m}_{e,l[n]} \right). \tag{5.10}$$

Implementing this in Simulink [3] and feeding the model with the input presented in section 5.3.1 one can estimate the heat transfer coefficient of the tank in equation 2.7 to

$$C_{BOG} = 0.337365.$$

A comparison of the model output tank pressure with the same input as the measured data and the measured tank pressure is presented in Figure 5-5. Figure 5-5 shows that the model follows the real tank pressure well, however since the effect of $\dot{Q}_{heat}$ is neglected the heat flow into the tank is much to high in comparison to the heat flow that is to be expected into the tank as derived in section 5.3.3, seen in Figure 5-6 where the BOG tank model is simulated for static operation, the rapid pressure drop spikes when the tank pressure reaches 16 bar is due to the opening of the BOV.

It is seen from Figure 5-6 that the BOVOT is much to low compared to the times presented in 5.3.3 only around 5 hours instead of 5 days. The simulation is done for a half full tank, for functional purposes since the model in not functional for stationary operation simulation for full tank simulation. This is again due to that $\dot{Q}_{heat} = 0$ removing the possibility for the model to describe the condensation of the vapour mass as seen in equations 5.9-5.10 and the dynamics related to this described in section 2.1.3. For high liquid levels, the vapour space is small, combined with the high heat flows from Figure 5-6 the pressure rise in the tank at stationary operation is too rapid and with the opening of the BOV, starts to oscillate and becomes unstable. It is hence concluded that the simplified BOG model cant be used for stationary operation simulation.

Varying the tank level for the mean mass flow of the measured mass flow in section 5.3.1 ($\dot{m}_e = 24.26$ % of max) out of the tank, as illustrated in Figure 5-7. Also indicates the problems with this modeling strategy for higher liquid levels in the

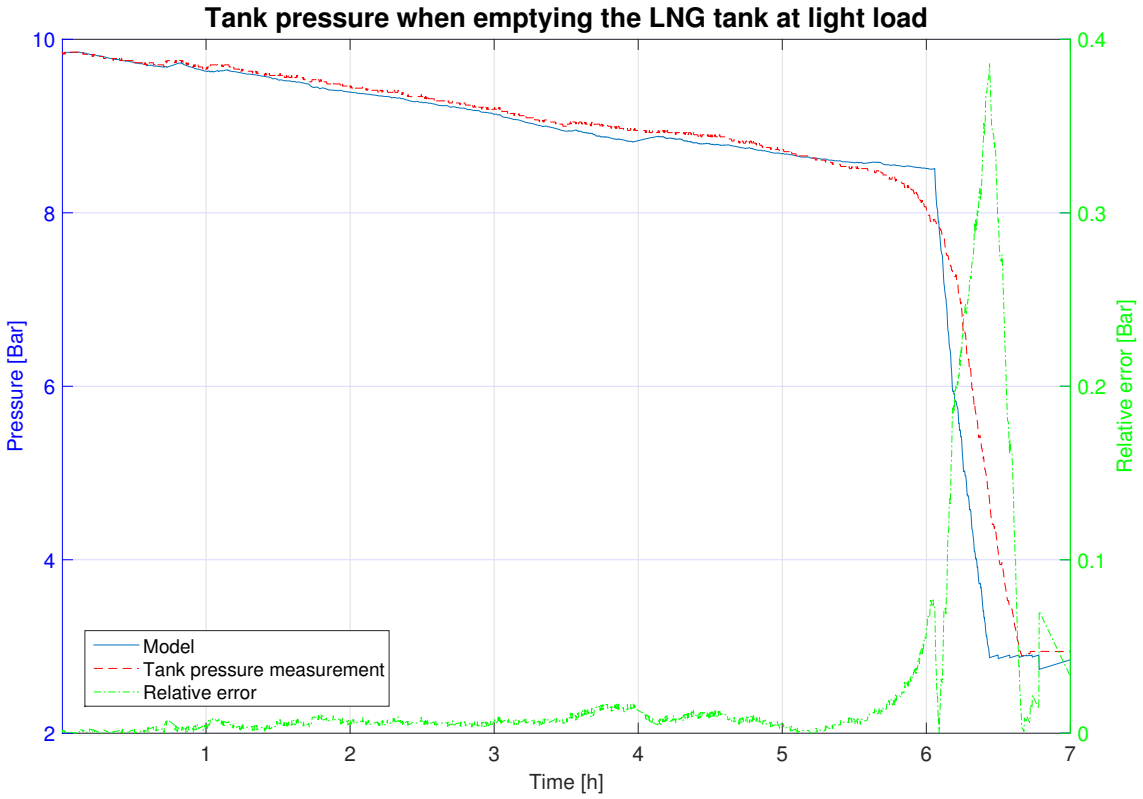

Figure 5-5: Comparison of the measured tank pressure and the model tank pressure for the simple BOG model. Initial tank level $level_{tank0} = 46\%$ and $p_0 = 9.85$ bar [3].

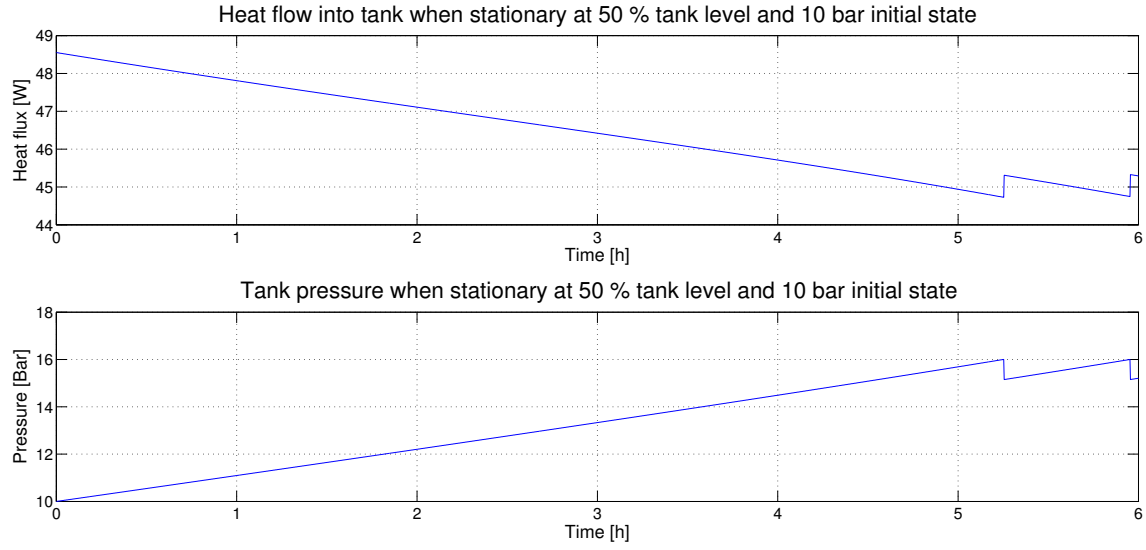

Figure 5-6: BOG model tank pressure and heat flow into the tank at stationary operation for initial tank level $level_{tank0} = 50\%$ and $p_0 = 10$ bar [3].

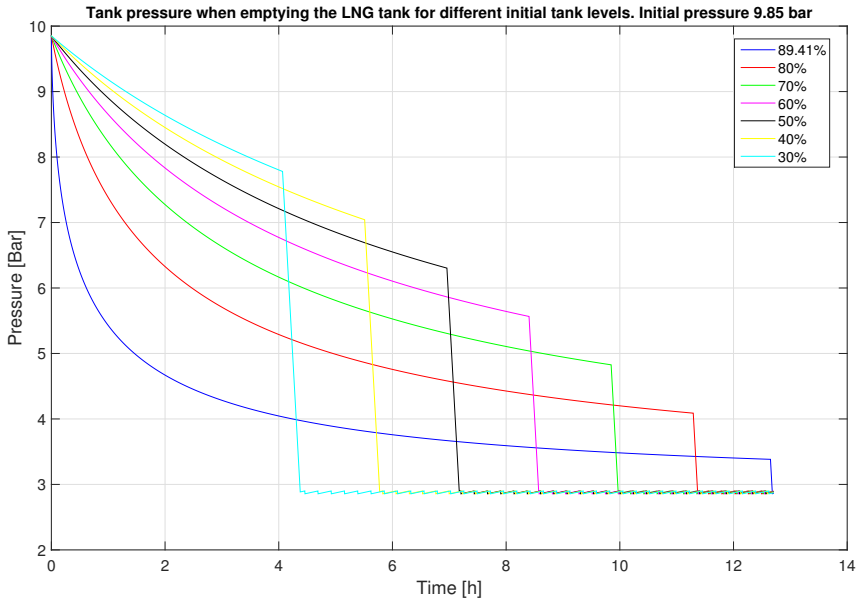

Figure 5-7: BOG model tank pressure for different initial tank levels $level_{tank0}$, with a mean engine consumption of $\dot{m}_e = 24.26$ % of max and $p_0 = 9.85$ bar [3].

LNG tank. Due to its inability to capture the linearity in the tank pressure drop when consuming liquid seen in the measured data in section 5.3.1 and 5.3.2 for any liquid level. It is hence concluded that the modeling strategy used for large LNG containers is not applicable for vehicular LNG tanks.

5.4.2 Model developed in the thesis

The primary modeling strategy used for the model developed in the thesis is the one that has been presented in Chapter 4. I.e. the heating of the cryogenic liquid and vapour is taken into account. Implementing the model state space equations 4.28, 4.29, 4.30, 4.31 and 4.32 in simulink [3] and also feeding this model with the data from section 5.3.1 the heat transfer coefficient from equation 2.7 is now estimated to

$$C = 0.12495.$$

Comparing the measured tank pressure in section 5.3.1 to the output of the model, Figure 5-8, one sees that it follows it well which is expected since C is based on this.

However when simulating the tank for static operation when filled to the manufacturers optimal filling point [6] as discussed in section 1.1.4 it can be seen in Figure 5-9 that this estimation of C agrees well with the data in section 5.3.3. Also it is seen from Figure 5-9 that the heat flow $\dot{Q}_{in}$ agrees better than with the indicated in 5.3.3. Running this model with the same input as the simplified BOG model, in the previous section, i.e. for half a tank fill it can be seen from Figure 5-10 that this type of modeling agrees a lot better with the hold times presented in section 5.3.3.

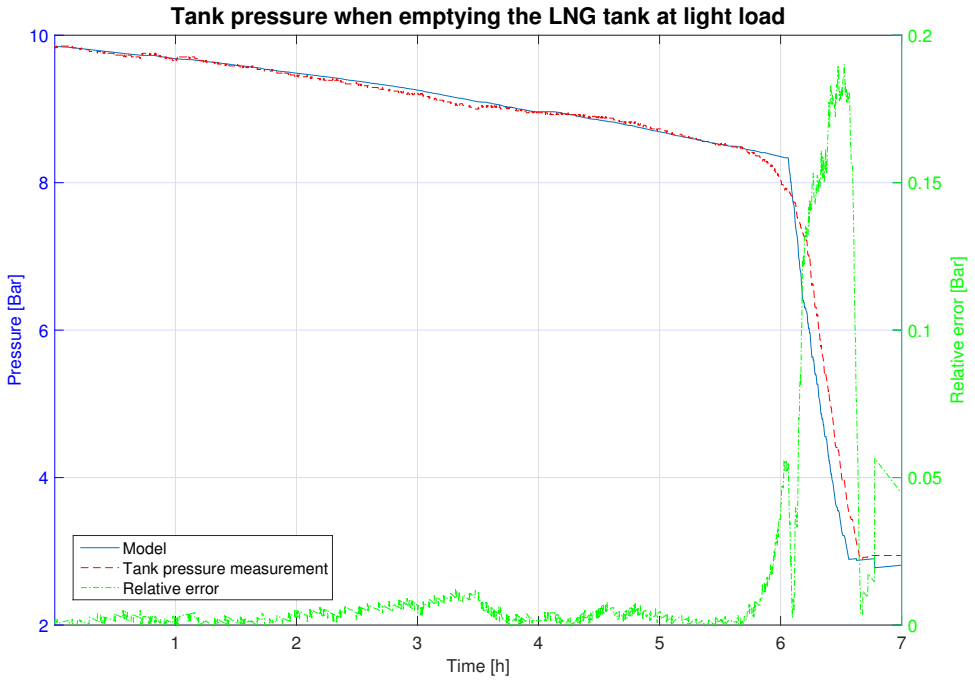

Figure 5-8: Comparison of the measured tank pressure and the model tank pressure for the model developed in the thesis. Initial tank level $level_{tank0} = 46\%$ and $p_0 = 9.85$ bar [3].

Furthermore in Figure 5-11 all the initial pressures for a full tank from Table 5.1 are simulated in the model. It is seen that the tank model hold time corresponds well with the lower of the initial pressures in Table 5.1, however for higher initial pressures it is seen that the hold time is longer than indicated in Table 5.1, agreeing with the reasoning of a safety margin at higher initial tank pressures in section 5.3.3.

Running a simulation with the same data presented in section 5.3.4 Figure 5-12 is obtained. It is seen that the pressure in the tank is estimated closer to the measured by the model developed in this thesis than the one developed in [4]. Using a smaller value of C from equation 2.7 than the one used in [4], would give better correspondence with the measured data with the model developed in the thesis.

Varying the initial tank level in this model with the same initial fill levels and initial pressure as in section 5.4.1. It is seen in Figure 5-13, that the behaviour of the developed model is of the same characteristic for all initial tank levels, as the measured data presented in section 5.3.1. This also agrees with what have been seen in initial measurements at Scania, like in the one presented in section 5.3.2 for full load.

Simulating with the full load data shows, in Figure 5-14, that the model is not catching some behaviour of the real system at full load. The behaviour is the same

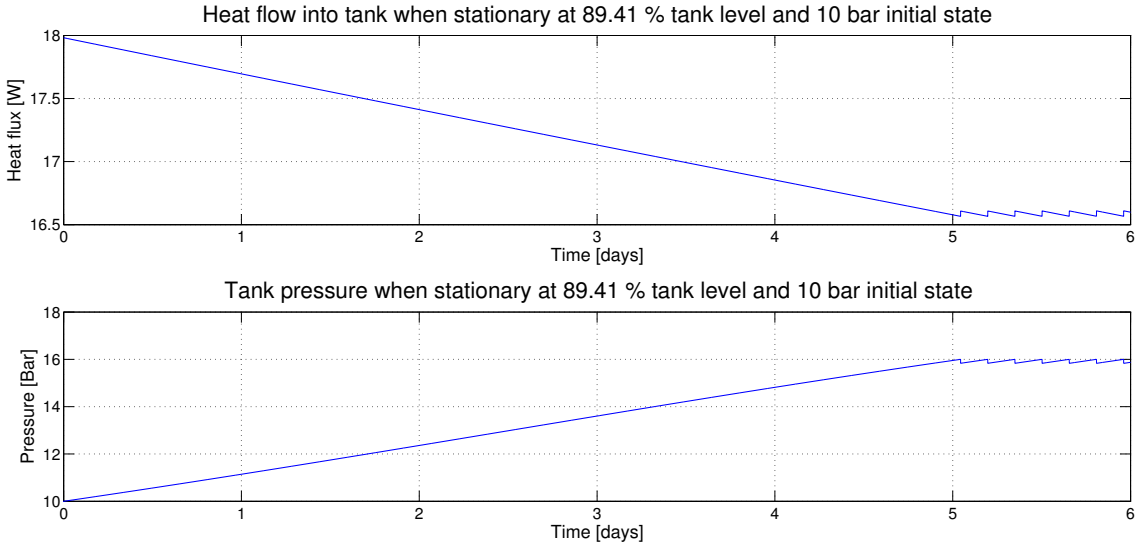

Figure 5-9: Thesis developed model tank pressure and heat flow into the tank at stationary operation for initial tank level at the tanks optimal hold time filling point $level_{tank0} = 89.41\%$ and $p_0 = 10$ bar [3].

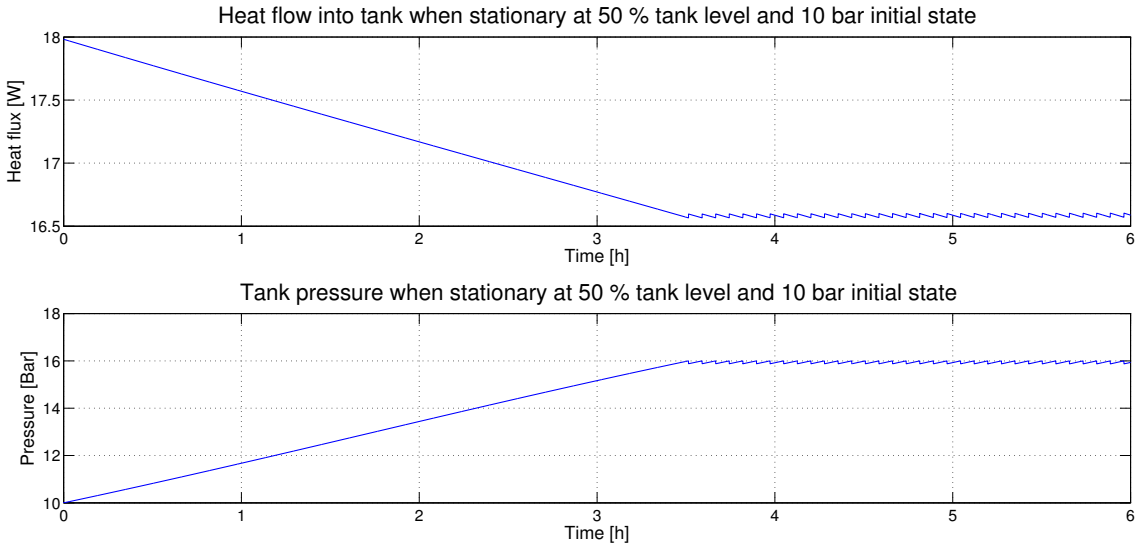

Figure 5-10: Thesis developed model tank pressure and at stationary operation for initial tank level of $level_{tank0} = 50\%$ and $p_0 = 10$ bar [3].

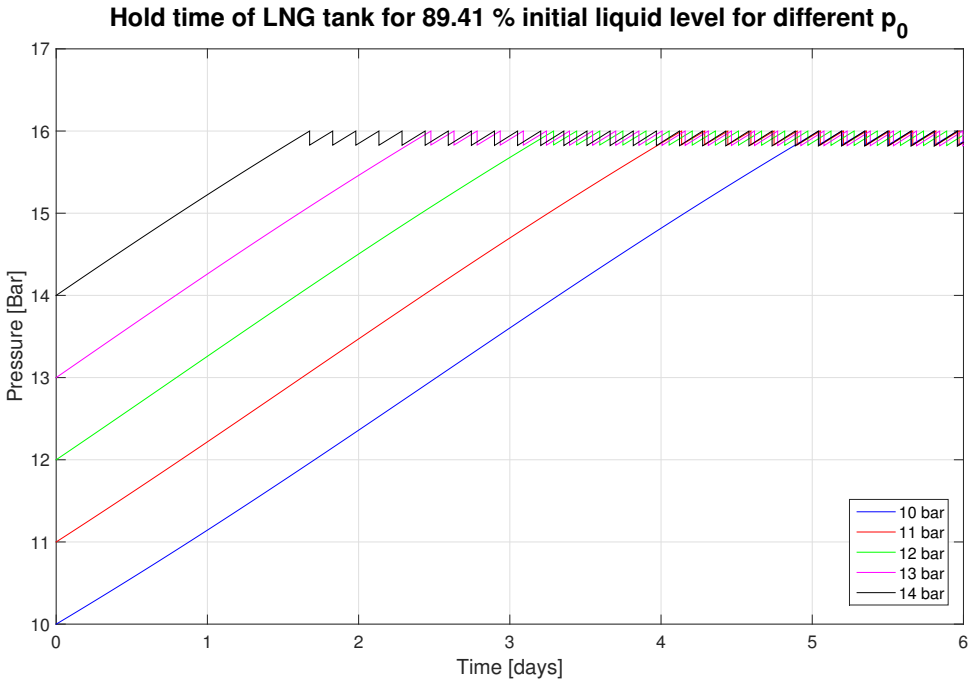

Figure 5-11: Thesis developed model hold time at stationary operation for initial tank level of $level_{tank0} = 89.41\%$ and initial pressures p_0 from Table 5.1 [3].

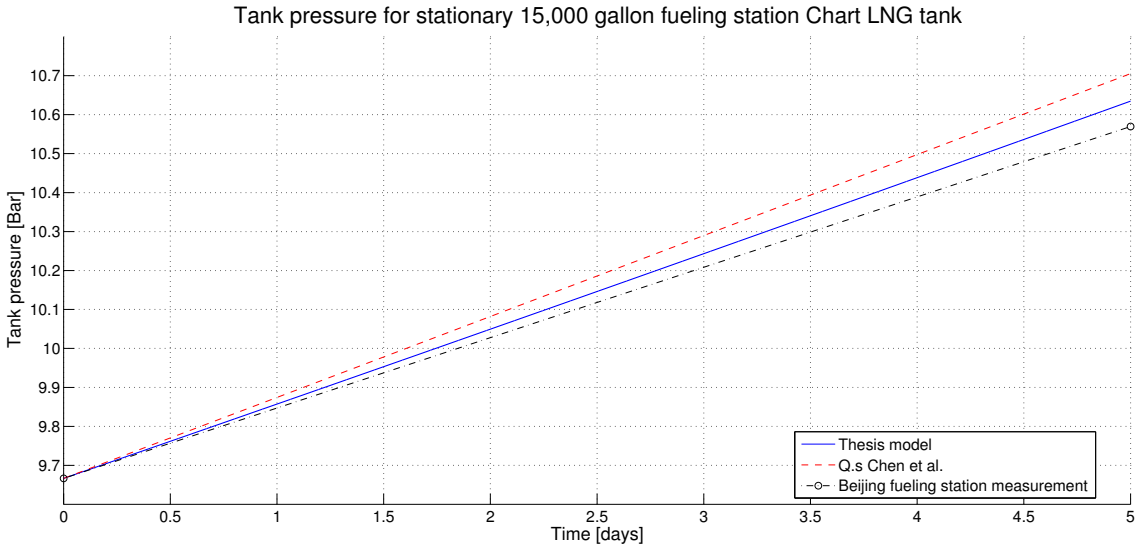

Figure 5-12: Comparison between measured tank pressure in a Beijing Fueling station LNG tank the model developed in [4] and the model developed in this thesis [3].

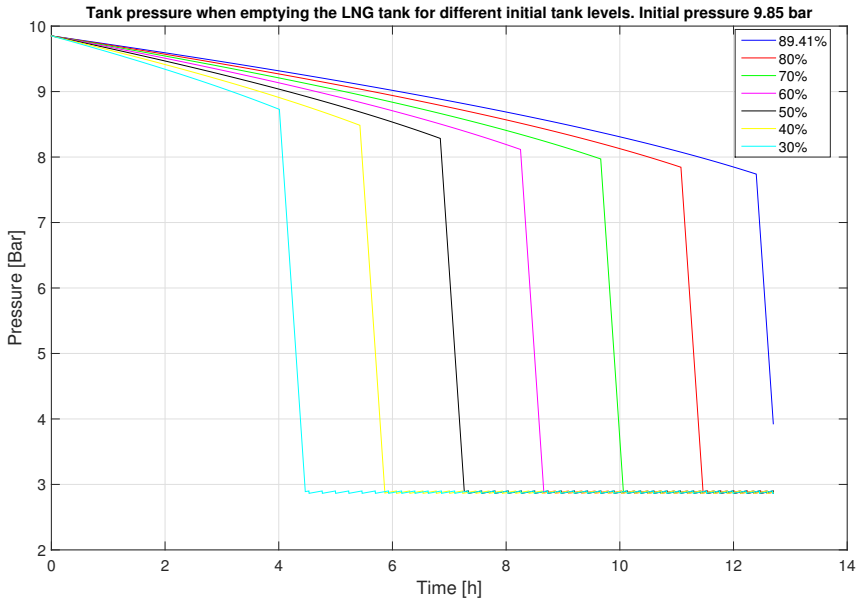

Figure 5-13: Thesis developed model tank pressure for different initial tank levels $level_{tank0}$, with a mean engine consumption of $\dot{m}_e = 24.26$ % of max and $p_0 = 9.85$ bar [3].

but the pressure drop is two slow. It has been proven with simulation that a lower $\dot{Q}_{in}$ gives a faster pressure drop. However, even setting this to 0 with the full load measurement data from 5.3.2 gives approximately the same behaviour as in Figure 5-14. The temperature is measured on the outside of the piping exiting the tank so an offset between model and measurement is expected as seen in Figure 5-14, making it unlikely that the behaviour is related to LNG composition. Furthermore it is seen from Figure 2-4 that the density for a low methane composition is increased by the higher dens hydro carbons. Making a faster pressure drop related to the extraction of liquid of lower density, an unlikely cause of this behaviour.

A more likely explanation is that a small vapour leakage through the Phase selector is present during the high mass flows $\dot{m}_e$ supplied to the engine during full load. Adding a vapour leakage through the Phase selector that is 40 times smaller than the consumed mass by the engine $\dot{m}_e$ during the consummation of liquid, shows better correspondence with the measured tank pressure from section 5.3.2 in Figure 5-15 I.e this indicate that some mix of vapour and liquid is fed through the fuel line at full load, indicating that the Phase selector is not completely digital in its operation in reality. The temperature dynamics also follows the dynamics of the measured better when adding a leakage as seen in Figure 5-15.

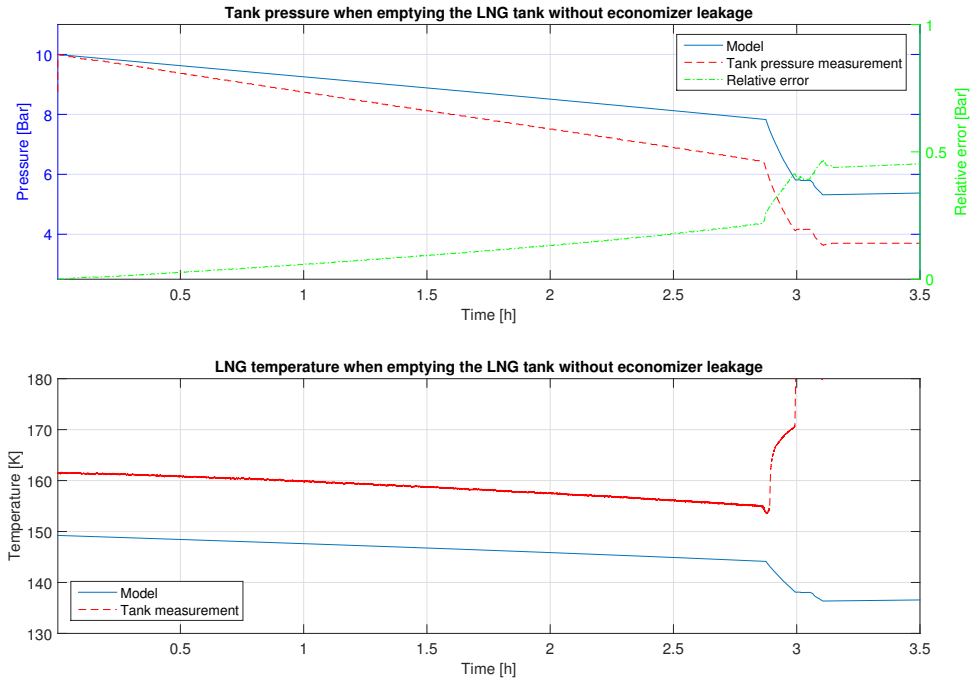

Figure 5-14: Thesis developed model simulated with the full load data in section 5.3.2 with the model implementation described in this Chapter [3].

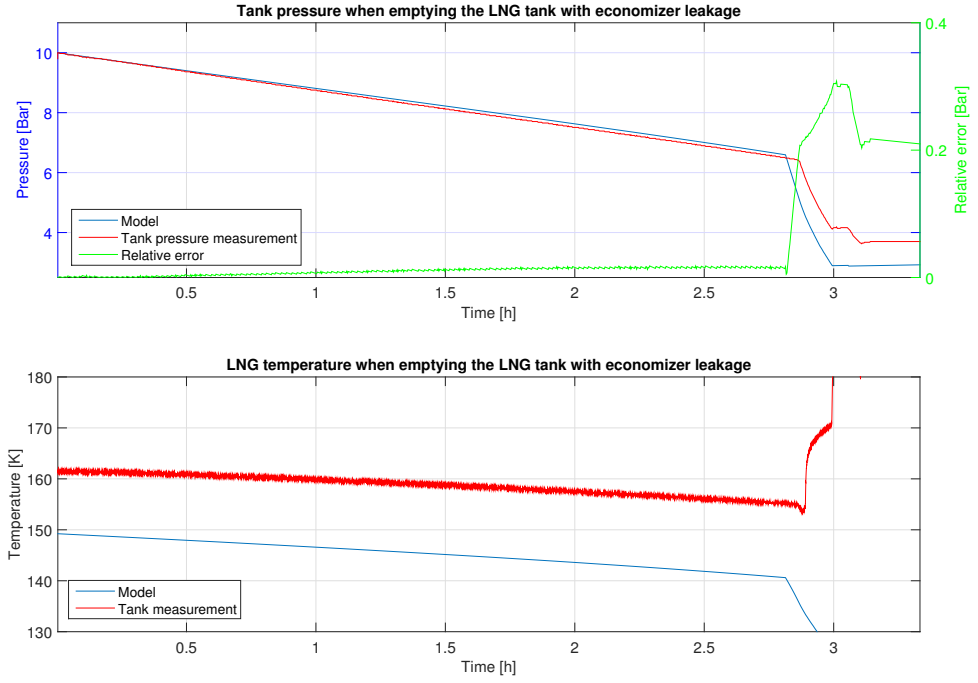

Figure 5-15: Thesis developed model simulated with the full load data in section 5.3.2 with an added Phase selector vapor leakage, during liquid fuel extraction [3].

5.5 Extended Kalman filter

In a model implementation on an embedded system if no correction of the model states is done with sensor data, a small error between the model and reality will due to the integral action of the state space equations 4.28-4.32, make the model drift and not estimate the sates of the LNG tank correctly. Therefore some observer that correct the model states with sensor data is required and a vast variety of choices are available but in the thesis a prof of concept extended Kalman filter is implemented in MATLAB and presented here in this section. This is due to the the Extended Kalman filters ability to estimate the states of a non-linear state space model dynamically with very noisy sensor signals, like the measurement signals in Figure 5-2, just by knowing the process and the sensor noise. The exact working principal of an EKF is not explained in the thesis since there exist a vast amount of literature and implementation examples on the subject, the theory of the EKF implemented is based on the literature in [29].

5.5.1 Algorithm used

An extended Kalman filter is an observer that estimates the current states x_k based on the process noise covariance Q and the measurement covariance noise R [29] of a non-linear discrete time state space

$$\begin{aligned} x_k &= f(x_{k-1}, u_{k-1}, w_{k-1}) \\ z_k &= h(x_k, v_k) \end{aligned} \tag{5.11}$$

Where the k and $k-1$ subscript represent the current and previous time step respectively, w_{k-1} and v_k represent the process and measurement noise respectively [29], z_k is the sensor measurement, f is the non-linear discrete time state space equations 4.28, 4.29, 4.30, 4.31 and 4.32. The non-linear function h is refered to as the measurement equation [29] and relates the states x_k to the measurements z_k. With some re-writing and assumptions in [29] one obtains the EKF time update equations

$$\begin{aligned} \hat{x}_k^- &= f(\hat{x}_{k-1}, u_{k-1}, 0) \\ P_k^- &= A_k P_{k-1} A_k^T + W_k Q_{k-1} W_k^T \end{aligned} \tag{5.12}$$

Where $\hat{x}_k^-$ is a *priori* estimate of the states in equation 4.1, $\hat{x}_{k-1}$ is a *posteori* estimate of the states at the previous time step, u_{k-1} is the input from equation 4.2 at the previous time step, A_k is the Jacobian

$$A_{[i,j]} = \frac{\partial f_{[i]}}{\partial x_{[j]}}(\hat{x}_{k-1}, u_{k-1}, 0), \tag{5.13}$$

P_k^- is the *priori* estimate error covariance, P_{k-1} is the *posteori* estimate error covariance at the previous time step, Q_{k-1} is in the implementation a diagonal matrix with

each states process noise in the diagonal, set constant. With the Jacobian of f with respect to w set to $W_k = I$ the calibrated process noise for each state only affect the state it was calibrated for in this implementation.

The EKF measurement update equations are with the same reasoning for $V = I$ so that only the sensor noise in the diagonal of R_k affect each sensor used by the EKF,

$$\begin{aligned} K_k &= P_k^- H_k^T (H_k P_k^- H_k^T + V_k R_k V_k^T)^{-1} \\ \hat{x}_k &= \hat{x}_k^- + K_k(z_k - h(\hat{x}_k^-, 0)) \\ P_k &= (I - K_k H_k) P_k^- \end{aligned} \tag{5.14}$$

where K_k is the Kalman gain and H_k is the Jacobian

$$H_{[i,j]} = \frac{\partial h_{[i]}}{\partial x_{[j]}}(\hat{x}_k^-, 0). \tag{5.15}$$

Iterating between equation 5.12 and 5.14 with an initial value of $\hat{x}_{k-1}$ and P_{k-1} with a desired sample time T_s gives the EKF estimation of the states $\hat{x}_k$ at each time step k which hence is T_s s long.

5.5.2 Numerical central difference Jacobian

Instead of computing the analytic Jacobians in equations 5.13 and 5.15 a central difference is computed for each entry in the Jacobian i.e.

$$J_{[i,j]} = \frac{\partial g_{[i]}}{\partial y_{[j]}} = \frac{g_{[i]}(y_{[j]} + h) - g_{[i]}(y_{[j]} - h)}{2h_{[j]}}. \tag{5.16}$$

Where h is a vector with the step length desired for each state central difference derivative. This implementation makes the EKF model independent with only the need to calibrate h. This means that changing the proposed relation between states in Chapter 4 to higher or lower order does not require re-design of the EKF implementation.

5.5.3 Observability

Following the reasoning in [30] the number of unobservable states of every linearization point can be derived by

$$O = \begin{pmatrix} CA \\ CA^2 \\ CA^3 \\ CA^4 \end{pmatrix}$$
$$s_{unob} = s - rank(O)$$

for a 5 state, state space, where O is the observability matrix, s_{unob} is the number of unobservable states, s the number of states in x, C is the linearization of $h(\hat{x}_k^-, 0)$ from equation 5.15 and A is the linearization of $f(\hat{x}_{k-1}, u_{k-1}, 0)$ from equation 5.13. If s_{unob} = 0, local observability is guaranteed, for the non-linear state space in every estimated point x_k. I.e. in the transient moving between linearization points observability can not be guaranteed. For all simulations in section 5.5.4, in every estimated point, the observability matrix O is computed with the linearized Jacobians A and H. For none of the linearization points is $s_{unob} \neq 0$ and hence the state space is locally observable in all linarization points.

5.5.4 Calibration and Results

The EKF is simulated with the measurement data for light and full load in section 5.3.1 and 5.3.2 and initialized with the initial measurements. First in Figure 5-16 the EKF is run with the Light load data, where the liquid level sensor, HPP pressure sensor and the engine consumption measurement is available. This is fed as sensor data and input respectively to the EKF and the measured tank pressure from the sensor in the tank is used as a reference for comparison in Figure 5-16. I.e. the measurement from the tank is not used by the EKF. There is an offset between the tank pressure and the pressure in the HPP due to pressure drops over components. This has been estimated to 0.7 bar and since the measurement is in gage the total offset is dp = 1.7 bar. Since the tank pressure is below 10 bar no Phase selector operation will be active, meaning that the pressure drop explained in section 3.3.2 is incorporated in dp. However this should be added as -0.14 if $\dot{m}_{e,l} \neq 0$ once the static pressure drop in the piping is known. The tank level measurement is calibrated according to section 5.3.1 and the function $h(x, u)$ that maps the states to the measurements hence become

$$h(x, u) = \begin{pmatrix} p - dp \\ V_l/V. \end{pmatrix}$$

It is assumed that the states of the tank do not vary considerably, so the process noise is estimated to

$$q = \begin{pmatrix} 1000Pa \\ 0.1K \\ 0.001m^3 \\ 0.005kg \\ 0.05kg \end{pmatrix} \tag{5.17}$$

which is the diagonal of the process noise covariance matrix Q. It can be seen from Figure 5-2 that both the HPP sensor and liquid volume sensor have a high amplitude of the sensor noise, so the sensor noise is estimated from the measurements to

$$r = \begin{pmatrix} 3Bar \\ 0.03m^3 \end{pmatrix}$$

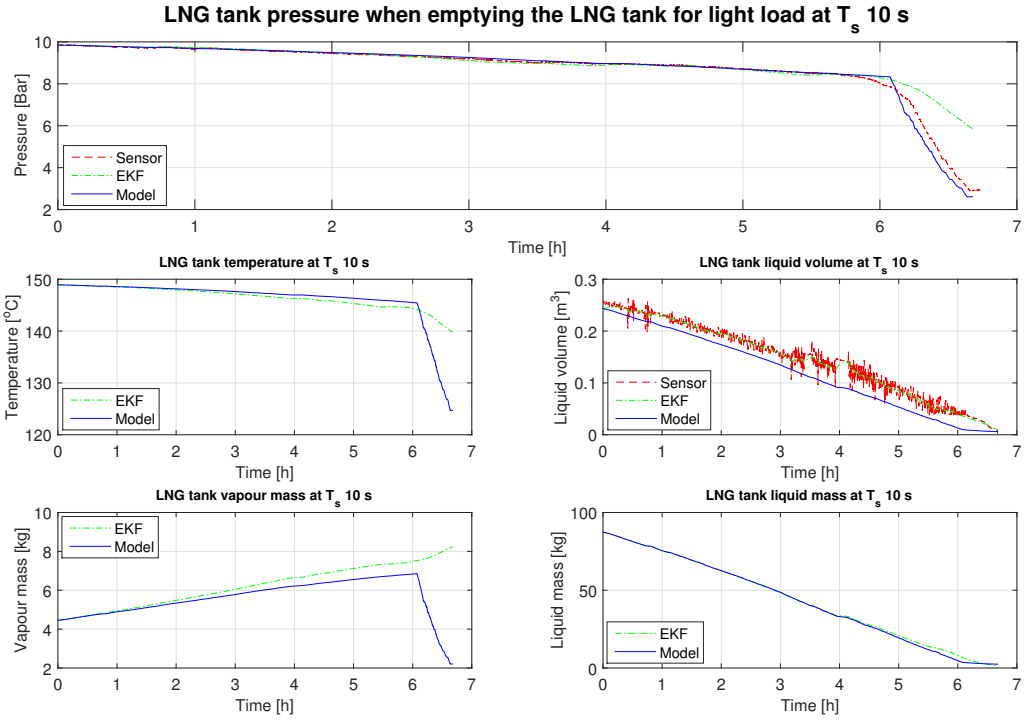

Figure 5-16: Simulation of the proof of concept EKF with measurement data available at light load at T_s 10 s [3].

which is the diagonal of the measurement noise covariance matrix R. The step length vector h is

$$h = \begin{pmatrix} 1000T_s \\ 0.1T_s \\ 0.0001T_s \\ 1T_s \\ 1T_s \end{pmatrix} \tag{5.18}$$

The initial guess of the P is a diagonal matrix with the diagonal q in equation 5.17. The initial states are computed with initial pressure $p_0 = 9.85$ bar and the initial liquid level 46 % from section 5.3.1. With all this and a sample time T_s of 10 s Figure 5-16 is obtained.

It is important to note here that the only state estimated by the EKF, that can be verified in this measurement is the pressure since the reference pressure measurement inside the tank is available for comparison for this state. The liquid state estimated by the EKF will follow the model or the liquid level measurement dependant on how the EKF is calibrated. The other states are only compared to the pure model estimation of the states and the comparison only shows the difference in estimation between the EKF and the model. It is seen that even at 10 s sample time and very noisy signals the EKF estimates the pressure well when liquid phase is consumed by the engine, but the slow sample time hinders it to converge when the tank is close to empty and the vapour phase is consumed. However changing the sample time to T_s

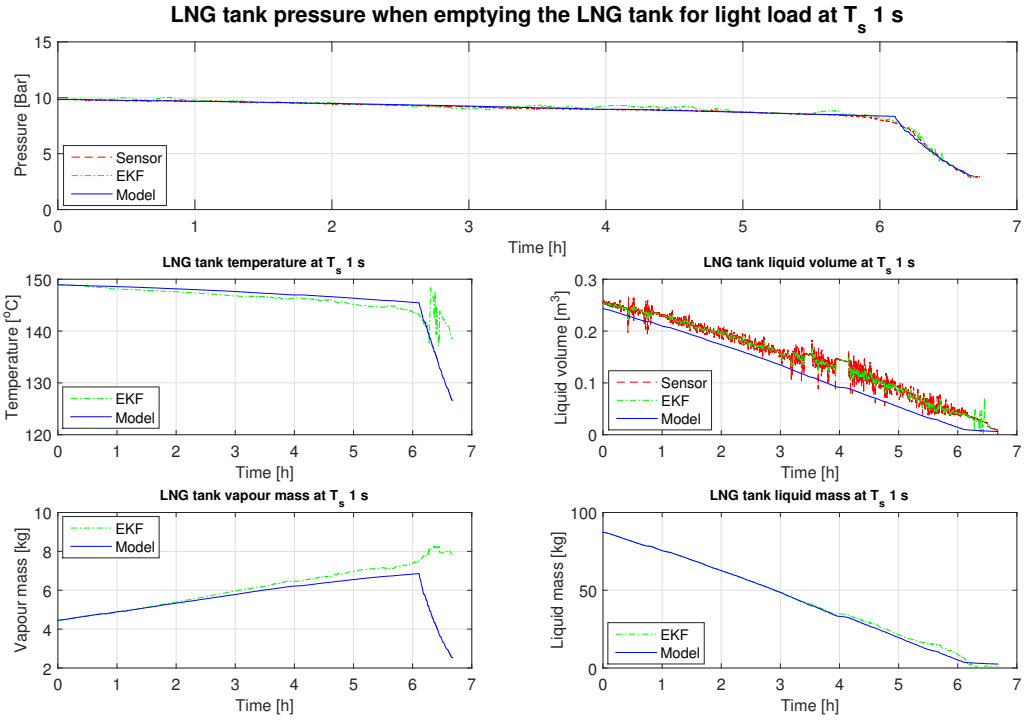

Figure 5-17: Simulation of the proof of concept EKF with measurement data available at light load at T_s 1 s [3].

1 s the performance of the EKF increases as seen in Figure 5-17 and the EKF estimates the pressure state close to the pressure measured in the tank during the whole measurement despite being corrected with the very noisy pressure measurement in the HPP.

For the full load measurement the same process noise and step length as for the light load is used i.e. equations 5.17 and 5.18. However in this data the only sensor data available is the the tank pressure measured in the tank and the temperature measured on the tank piping. The tank pressure is not gauge i.e. relative vacuum and from a comparison between Figure 5-4 and the model an offset of $dT = 13$ K is identified. The state to measurement equation hence becomes

$$h(x,u) = \begin{pmatrix} p \\ T \quad +dT \end{pmatrix}.$$

The noise level on these sensors are relatively small so r for the full load simulation is estimated to

$$r = \begin{pmatrix} 0.1 & Bar \\ 0.2 & K \end{pmatrix}$$

With the initial pressure p_0 10 bar, the initial tank level of 60 % and sample time T_s of 10 s, Figure 5-18 is obtained. Since the EKF is corrected with the tank pressure measurement, with low both sensor and process noise the estimation will be close to

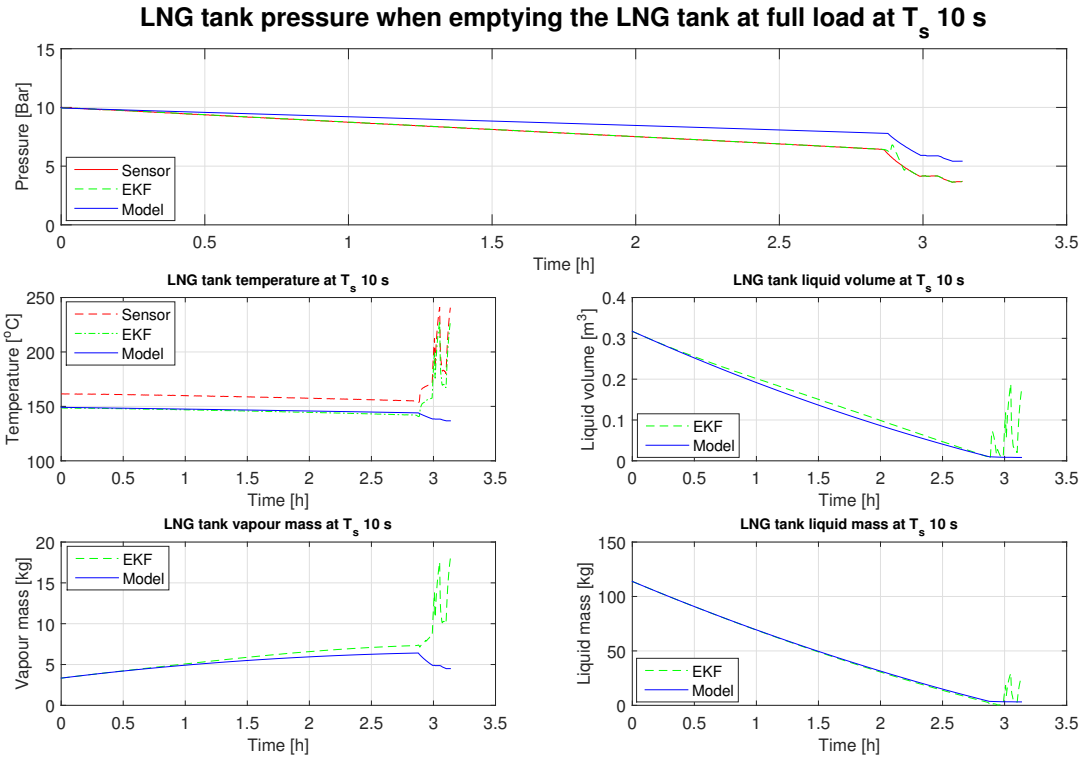

Figure 5-18: Simulation of the proof of concept EKF with measurement data available at full load at T_s 10 s [3].

the measurement which is desired. However, since the tank pressure is to be estimated with a measurement in the HPP (unavailable in this measurement) in an implementation, this does not verify the usage of the EKF at full load for estimation of the tank pressure. It is hence concluded that further measurements with the required sensor data needs to be performed at full load to verify the EKF in this operation mode.

Despite of this, since the EKF follows the tank pressure measurements and the temperature of the model as seen in Figure 5-18, the effect of this can be analysed for the remaining states. It is seen that the EKF estimates the liquid volume higher than the model, due to the higher estimated BOG added to the vapour mass m_g from the liquid mass m_l. It is the faster pressure drop making the EKF estimate a less dense liquid extracted from the tank that is the reason for the divergence of the states V_l, m_g and m_l. However as mentioned in section 5.4.2, the faster pressure drop is more likely to the leakage of vapour mass through the Phase selector , meaning that additional functionality is required for the usage of the EKF during full load operation.

Chapter 6

Analysis and Future work

In this Chapter the developed vehicular LNG tank model and the EKF is analysed, in regard to implementation and their load on an embedded system is derived. Future work and improvements of the developed material is suggested and the research questions of the Master thesis is answered.

6.1 Model analysis

This section aims to answer research question 1, analyse the developed model and suggest future possible improvements of the vehicular tank model.

6.1.1 Heat transfer coefficient

The largest uncertainty in the model developed in the thesis is the heat transfer coefficient C in the linear, one dimensional heat transfer model in equation 2.7. Now using the linear heat transfer model the developed model follows the measurement data well. But since the measurement data is from vehicle operation of the tank, the heat flow $\dot{Q}_{in}$ is very small in comparison to the energy removed from the system with the liquid and vapour mass consumed by the engine. For example by setting $\dot{Q}_{in} = 0$ in the full load simulation in Figure 5-14, almost no difference in the model response is seen. Since the value of C is verified against only indicative data from the tank manufacturer the verification is uncertain. Meaning that in a simulation of the hold time, it can not at this stage be guaranteed that the BOVOT from the model would be correct. The estimation of C needs to be quite precise to achieve an exact prediction of the BOVOT, due to the very long hold times of LNG tanks, making a small error in the heat flow reaching the cryogenic system result in large errors in time. Furthermore as explained in section 2.2.3 the major source of heat entering the tank is through the metallic connection between the outer and inner shell. Since there is a factor of 10 between the heat conductivity between the liquid and vapour phase [2]. The liquid level in the tank should affect the heat transfer coefficient C making it larger for liquid levels near and over the metallic contact. The vapour cooling of the piping submerged into the LNG, dependence on liquid level, as discussed in section

2.2.2, could also affect C.

This should be determined by a long measurement on the tank during stationary operation for these different liquid levels. If the level is proven to affect C, a condition on C should be implemented in the developed model or if proven to not be of digital nature, when the liquid level passes the metallic contact, some more complex heat transfer model will be required desirably as a function of liquid level since this measurement is available. Also since $\dot{Q}_{in}$ affect the model little during high engine consumption and that the states of the system change slowly. On line estimation of this constant with for example the suggested EKF, is not recommended since it can only be done for low mass flows $\dot{m}_e$ and even then the small state variations over time might be hard to measure and relate to $\dot{Q}_{in}$ due to process and sensor noise. It is hence concluded that more research through measurements is required to verify the model simulation of the hold time of the LNG tank.

6.1.2 Developed model analysis

It is proven in section 5.4.1 that the heating of the cryogenic liquid and vapour phase needs to be considered, for the model to be able to function, in the wide pressure range of the tank. Therefor it is concluded that when modeling a tank with a much wider pressure range, than the larger LNG tanks discussed in 5.1 that this physical phenomenon needs to be incorporated in a model of a vehicular LNG tank. It is also concluded that the developed model is not able to function with solely a single phase (it is singular for this situation) and need to be expanded for this situation as explained in section 5.2.5. However it is not recommended that this is done since the situation when all liquid in the LNG tank has been consumed is not a realistic operating case. This since at low liquid levels the engine will consume the vapour phase as explained in 3.3.3 and due to the long hold time of the tank, evaporation to raise the tank delivery pressure to the required by the engine, will take a long time and not give any reasonable range, so that the truck can be driven to a fueling station. Also a tank that has been completely emptied require a special fueling procedure [6]. Since once the LNG is not present the major thermodynamical resistance of the system is removed and the tank temperature will converge to ambient much faster. Due to these reasons it is instead of adding an additional single phase model, suggested that the driver is warned well in advance that fueling is required so that the single phase operation state is avoided in the tank. In section 2.3 it is assumed that the LNG consist of 100 % methane, since the composition of the fuel in the verification of the model is not known it can not be concluded that this assumption is valid. However with the reasoning in that section and the close correspondence of the model to the measurement data in section 5.4.2 one can assume that this assumption is valid and that no consideration to the composition of the LNG, in the modeling of the tank states, needs to be taken.

6.1.3 Models of auxiliary components

The model used for the BOV is already discussed in section 5.2.4 and the conclusion is that it should not be implemented in real application. It is instead suggested to trust the sensor data to a greater extent if the opening of the BOV against all odds should occur. The algorithm of initializing all states from only two measurements is a very effective way to reduce the amount of sensors needed for model initialization. However this makes the model initialization sensitive to error in theses two measurements, since an error in the measurements will propagate through all states because all states are based on these measurements, this further motivates the usage of an observer that filters out measurement uncertainties in an ECU implementation.

In section 5.4.2 it is concluded that some leakage of vapour mass is present during high liquid mass flows out of the tank, most likely through the Phase selector . Furthermore as concluded in section 5.5.4, to be able to use the prof of concept EKF at this tank operation. Additional functionality needs to be added to Phase selector cases in 5.2.2 dependant on the fuel consumption. If the cases in 5.2.2 would be replaced with a dynamical model of the choice of the phase extracted from the tank, the model will most likely also catch the smother transition from the consumption of liquid phase, to the consumption of vapour phase seen in Figure 5-8. It is seen in Figure 5-14 that the divergence from the real pressure is almost instant, furthermore in Figure 5-18 it is seen that the EKF removes this behaviour. This means that either an a mass flow dependant leakage can be added to the cases in 5.2.2 where the dependence is adapted with the EKF or that the parameters of a dynamical replacement model could be identified on line. Making the model application robust against component degradation over time. Allowing for long service time, state estimation of a vehicular LNG tanks states.

6.1.4 Final remarks model

A new way to model a cryogenic LNG tank is suggested in the thesis, by introducing the concept of a saturated system and the description of such a system with low order analytic functions. Also the concept of modeling larger LNG tanks, which is the most common as explained in 5.1, is applied to a vehicular tank with a much wider pressure range and concluded to be insufficient. A model over the vehicular LNG tank have been developed in the thesis and it corresponds well with measured data from the real tank and the accuracy is seen in the Figures of section 5.4.2. Since LNG is a new concept in vehicular application it is not known what model accuracy is required in different vehicular LNG applications, therefore it can not be concluded if the accuracy of the model is too high or too low. However since the relative error of the tank pressure is in the range 0.2-0.3 bar maximum at light and full load (with the suggested leakage functionality) and this is in the same range as the error of an industrial pressure sensor, one can assume that this accuracy is sufficient for most applications. Furthermore if an EKF is used, high accuracy of the model is less important, instead it is important to know the accuracy in that case so it can be

supplied to the EKF as the process noise so that the EKF can estimate the real state based on this. The most important factors to consider in the modeling is discussed in section 6.1.2. Hence research question 1 have been answered. Some improvements are suggested all adding to the computation time discussed in the next section.

6.2 Computation time analysis

In this section an analysis of the computation time of the model developed in the thesis is performed. The two different implementation strategies suggested in section 4.4 is compared and research question 2 and 4 is answered.

The CPU instruction required by each array look-up operation of course depends on the implementation of the look-up algorithm and the size of the data array. Why an exact comparison between an analytic and look up table implementation only can be done for two specific implementations. Since no look up table implementation have been developed in the thesis, such a comparison will not be performed. However some general differences between these forms of implementation is discussed in section 4.4 and some additional will be discussed here. Also an approximation of the computational time for one iteration of the LNG tank model discrete time state space in section 4.10, is performed on a relative high performance general industrial embedded system CPU [7]. This system has a maximum clock frequency of 80 MHz which will be assumed to be used in the calculations below. Furthermore it will be assumed that each instruction (ins) takes one clock cycle without any latency or additional overhead. No regard to the handling of floating points will be considered, neither will data types be specified for the variables, instead the worst case for integers are used, since no analysis of required/optimal data types have been performed in the thesis. The CPU instructions required for the required operations on fixed points by the model is seen in Table 6.1. It is also assumed that every math operation requires one store operation of the result of that operation. It is assumed that the computation of the power of two require one additional storage operation i.e. 3 instructions total. That the power of three requires two additional storage operations i.e. 5 instructions total. This is also added to Table 6.1. The reading of the input data is assumed to be one load operation.

6.2.1 Computation time of the model

With the help of table 6.1 with a worst case scenario of large data types i.e. 16 instructions for a division operation. The total number of instructions required to run the model in section 4.10 one iteration can be calculated. As seen from equations 4.20, 4.14, 2.6 and 2.7 that the required instructions for the computation (comp) of

Table 6.1: Required instructions for integer operations on a relative high performance general industrial embedded system CPU [7]

.

Operation	Instructions
Add/subtract	1 + 1
Multiply	1 + 1
Divide	6-16
Store/Load	1
Compare/logical	1
power of 2	3
power of 3	5

each parameter is

$$\begin{aligned} L_v comp_{ins} &= 12 \\ k_p comp_{ins} &= 16 \\ R comp_{ins} &= 7 \\ \dot{Q}_{in} comp_{ins} &= 6 \\ parameters_{Totins} &= 41 \end{aligned} \tag{6.1}$$

Equation 4.28, the next state of p, consist of

$$\begin{aligned} add/subtract_{op} &= 8 \\ multiplication_{op} &= 19 \\ divide_{op} &= 1 \end{aligned}$$

operations (op) assuming $V - V_l$ is only computed once and that static constants and state variables are accessible without any additional instructions. All the parameters in equation 6.1 needs to be computed in equation 4.28 so with Table 6.1, the required instructions to calculate $p_{[n+1]}$ is

$$p_{[n+1]} comp_{ins} = 41 + 8 \times 2 + 19 \times 2 + 1 \times 16 = 111.$$

In equation 4.29 most is already calculated so the next state of T requires

$$\begin{aligned} add/subtract_{op} &= 1 \\ multiplication_{op} &= 2 \end{aligned}$$

operations and

$$T_{[n+1]} comp_{ins} = 1 \times 2 + 2 \times 2 = 6$$

instructions. Looking at equations 4.31 and 4.32 it is seen that both equations require exactly the same amount of operations

$$\begin{aligned} add/subtract_{op} &= 3 \\ multiplication_{op} &= 2 \\ divide_{op} &= 1. \end{aligned}$$

Also the reading and determination of the input $\dot{m}_e$ by the conditions in the cases 5.4 require

$$\begin{aligned} Load_{op} &= 3 \\ Compare_{op} &= 2 - 10 \\ Store_{op} &= 2 \end{aligned}$$

operations, for the worst case when all conditions in the cases 5.4 need to be evaluated, the instructions required to compute the mass states are

$$m_{g+l[n+1]}comp_{ins} = (3 \times 2 + 2 \times 2 + 1 \times 16) \times 2 + 3 \times 1 + 10 \times 1 + 2 \times 1 = 67.$$

In equation 4.30 it is seen that

$$\begin{aligned} add/subtract_{op} &= 2 \\ multiplication_{op} &= 4 \\ divide_{op} &= 2 \\ power2_{op} &= 1 \end{aligned}$$

operations are required to compute the liquid volume state and hence

$$V_{l[n+1]}comp_{ins} = 2 \times 2 + 4 \times 2 + 2 \times 16 + 1 \times 3 = 47$$

instructions. Saturating one state between two limits, two state with only one limit and in the worst case writing the saturation limit to all three states require

$$\begin{aligned} Compare_{op} &= 4 \\ Store_{op} &= 3 \end{aligned}$$

operations and

$$saturate_{ins} = 4 \times 1 + 3 \times 1 = 7$$

Saving all 5 states to static variables require 5 store operations making it a total of

$$StateSpacecomp_{ins} = 111 + 6 + 67 + 47 + 7 + 5 = 243$$

With one clock cycle per instruction and 80 MHz clock frequency the computation time for the worst case scenario of the model is 3.0375 μs meaning that the processor load of the model running as a cyclic 10 ms application would be 0.03 % which is

very low leaving 99.97 % free for observer functionality and safety critical applications. However it has been shown in Chapter 5 that the Extended Kalman filter can be run at T_s 10 s with good estimation accuracy at slow system dynamics. With this cycle time the processor load can be neglected since it is 0.3 10^{-4} %. It is concluded that a computational effective model has been developed that does not lock the processor in model computation as required in Chapter 1. Hence Research question 4 have been answered and the processor load is 33 times lower for a high precision computational cycle of 10 ms and 33 333 times lower for the 10 s computational cycle witch gives high accuracy results in Chapter 5.

6.2.2 Analysis of BOVOT estimation

To avoid the release of BOG resulting in a flammable mixture with air, on ferries and in other confined spaces. It is desireable to introduce, in all NGV with an LNG fuel system, BOVOT estimation functionality that informs the driver the remaining time to the opening of the BOV so that the release of BOG can be avoided. This is also important for future pressure control in the LNG tank, where the estimation functionality can be used in the reversed way, so that the driver sets a desired hold time of the tank and the pressure is regulated down to the pressure giving such a hold time.

For a very simple implementation of the estimation of the BOVOT, as iterating the discrete time state space with sample time 10 s as simulated in Figure 5-9. With a compare operation of the BOV opening pressure and the simulated tank pressure p, the addition of the elapsed time to a static variable for each iteration, the computation time is 3.075 μs. Assuming the BOVOT would be 5 days, with T_s = 10 s, 432 000 iterations would be required and the simulation would hence take 1.33 s if the CPU is locked for this calculation only, which is not desirable for such a long time. To not lock the processor at a 10 ms cyclic application at T_s 10 s, the simulation time would hence be 1.2 h. This is not possible to use in an application, therefor the results of simulations for different sample times T_s is seen below in Table 6.2, where the reference estimated BOVOT is the one obtained at T_s = 1 s. Furthermore in Table 6.2 is the result of an estimation by the algorithm in equation 6.2 [31]

$$t_{BOVOT} = \frac{p_{BOV} - p_0}{dp_{[0]}} \tag{6.2}$$

Where $dp_{[0]}$ is the pressure derivative in equation 4.28 evaluated at the initial states, p_{BOV} the BOV opening pressure and t_{BOVOT} the estimated BOVOT. This algorithm is equation 4.28 rewritten and one step is taken [31] i.e. the BOVOT is the sample time, hence it require a lot less computational time, since in the simulations, the required iterations decrease by 10 when T_s is increased by 10. The initialization algorithm from section 5.2.1 require 56 instructions and hence it is seen from equation 6.2 that the total instructions are $t_{BOVOT}comp_{ins} = 183$ and hence a computation time of 2,29 μs.

It is seen from Table 6.2 that the estimation algorithm for one iteration, has

Table 6.2: Results of different BOVOT estimation strategies for different sample time T_s and resolution (n_r). Calculation times compared for 100 % processor load and p_0 = 10 bar, $level_{tank0}$ = 89.41 % (full) and T_{amb} = 20 ^{o}C.

T_s/n [s/res]	BOVOT [days]	Error t	Error p [Pa]	Calc. time
$T_s = 1$	5.0005	N/A	N/A	13.3 s
$T_s = 10$	5.0005	1 s	1.3	1.33 s
$T_s = 100$	5.0012	61 s	77.9	133 ms
$T_s = 1000$	5.0116	16.02 min	1220	13.3 ms
$T_s = 10\ 000$	5.0926	2.21 h	10 140	1.33 ms
$T_s = 100\ 000$	5.7870	18.88 h	86 400	0.133 ms
$n_r = 1$	5.4424	10.61 h	N/A	2.29 μs
$n_r = 10$	5.0054	7.12 min	N/A	23.2 μs
$n_r = 100$	5.0023	2.64 min	N/A	231.5 μs
$n_r = 1000$	5.0024	2.78 min	N/A	2.32 ms
$n_r = 10\ 000$	5.0024	2.80 min	N/A	23.2 ms
$n_r = 100\ 000$	5.0024	2.80 min	N/A	231.5 ms

approximately the accuracy between the $T_s = 10\ 000$ s and $T_s = 100\ 000$ s simulations, but considerable less computational time. The resolution of the algorithm in equation 6.2 can be increased by making multiple steps as

$$t_{BOVOT} = \sum_{i=1}^{n_r} \frac{p_i - p_{i-1}}{dp_{[i-1]}} \tag{6.3}$$

[31] where the resolution is n_r, p_{BOV} is the n:th pressure and naturally the computation instructions increase by $n_r(t_{BOVOT}comp_{ins} + 2)$ as seen in Table 6.2. It is seen from Table 6.2 that the optimal resolution of the algorithm in equation 6.3 is n_r = 100 and the computational time is only 0.23 ms i.e a processor load of 2.3 % in a 10 ms application.

It is concluded that for approximately the same, shorter sample times, the simulation estimation is a better BOVOT estimator however the algorithm from equation 6.3 is more accurate at longer sample times. The algorithm is also a lot more computationally effective, since all states from the state space of section 4.10 is not computed every iteration, this is also why the accuracy is worse, since the dynamics of the state space is replaces by initialising the states at each iteration.

The intended BOVOT estimation functionality does not require perfect accuracy since at minute basis the model error and error in estimating the heat transfer coefficient C will affect the estimation of the BOVOT. Therefore the sample

times/resolutions that give minute base BOVOT estimation errors are recommended to be used in a real application. I.e. the requirement on the BOVOT estimation application should be that the error should not be greater than 1 h to avoid boil-off valve opening on ferries and in other enclosed spaces. Also it is not desirable to have to great safety margin on the estimated BOVOT, since it could create bad-will, if the customer would after the estimated BOVOT look at the tank pressure gauge and see that the tank pressure is not close to 16 bar at all, hence causing the driver to lose faith in the BOVOT estimation.

6.2.3 Comparison of analytic and look up table implementation

The state relations in equation 4.9, 4.10 and 4.12 on differential form is

$$p = f_1'(\rho_g)\dot{\rho}_g, \tag{6.4}$$

$$T = f_2'(p)\dot{p}, \tag{6.5}$$

$$\rho_l = f_4'(T)\dot{T}. \tag{6.6}$$

As mentioned in sections 4.6, 4.8 and 4.9 and using the methods in these sections to derive the state equations it is seen by comparing the form of equations 4.25, 4.14 and 4.22 to 6.4, 6.5 and 6.6 that

$$a_\rho = f_1'(\rho_g), \tag{6.7}$$

$$k_p = f_2'(p), \tag{6.8}$$

$$a_T = f_4'(T). \tag{6.9}$$

This means that inserting 6.7, 6.8 and 6.9 into the discrete time state equations in section 4.10 gives the general expression for any implementation of the description of the saturation properties relation between the states. Implementing data maps as discussed in section 4.4.2, f_i' in equations 6.4, 6.5 and 6.6 would be implemented as some numerical difference like Euler forward, backward or as a central difference. On the form

$$f_i' \approx \frac{f_i(x+h) - f_i(x)}{h}$$

for example for Euler forward. Meaning two data array look-ups, one subtract (sub) and a division in the worst case scenario. Meaning that the additional instructions required for computation of a look up table implementation in equations 6.7 and 6.9 instead of the linear analytic relations, in the state space equations in section 4.10 are

$$additional_{ins} = 2 \times lookUp_{ins} + sub_{ins} + division_{ins}.$$

Since k_p is not a constant as in the linear case and requires computation, the additional instructions for the look up table implementation in in equation 6.8 is

$$additional_{ins} = 2 \times lookUp_{ins} + sub_{ins} + division_{ins} - k_p computation_{ins}.$$

This would of course also be the case in equations 6.7 and 6.9, were f_1' and f_4' of higher order. L_v in equation 4.20 is not time differentiated and would therefore only require one table look-up

$$additional_{ins} = lookUp_{ins} - L_v computation_{ins}.$$

On the CPU used for the analysis in section 6.2, a division operation require 6 to 16 CPU instructions dependant of data type [7]. Meaning that in some best case scenario for 8-bit variables and only one instruction for the look-up operation, the look up table implementation would still require a total of 3 instructions more than the model implemented with analytic function. A look-up operation of 1 instruction is unreasonable, a more realistic, neglecting interpolation and only stepping in one direction, would be

$$lookUp_{ins} = (load_{ins} + compare_{ins} + pointer{+}{+}_{ins} + index{+}{+}_{ins}) \times n + loadTableData_{ins}.$$

Where n is the steps in the data array and ++ is a add/subtract operation. With data from Table 6.1 for the desired data at the end of a data array of lenght 20, $lookUp_{ins} = 121$ i.e. $Totadditional_{ins} = 843$. Hence the implementation in section 4.10 is more computational effective regardless of the look-up algorithm used in a look up table implementation.

Regarding memory usage, it is elementary to see from equations 4.24 and 4.21 that the linear analytic functions require two static variables of data type size of storage on the RAM during ECU operation. From equations 4.13, 4.20 and 2.6 it is seen that four, three and two statics are required respectively also T_s, C and V. Also each state need to be stored as static variables. I.e. a total 21 statics whereas the look up table implementation require

$$2\sum_{i=1}^{4} n_i + 5 + 5$$

static variables for all data maps f_i in equations 4.9-4.12 and the constants required in both implementations. Meaning that the *total* length of the arrays of the four data maps f_i must be less than 11 long witch is highly unlikely for the same accuracy as the analytic implementation, if a look-up algorithm as the one suggested earlier. It is hence concluded that the analytic implementation is more computational and memory usage effective than the look up table implementation.

6.2.4 Final remarks Calculation comparison

It has been shown that the most computationally effective model implementation is the analytic function implementation. It is proven in Chapter 5 that the heating of the liquid is required to be incorporated in a vehicular tank model to be able to function. The model proposed in section 4.10 is therefore the most optimal implementation strategy when running the model on an embedded system. The initialization of the model require two sensor data according to section 5.2.1 and the minimum amount of sensor required by pure model operation is two (which is also the case for the suggested prof of concept EKF). The minimal required computing power depends on acceptable processor load, assuming 70 % as the maximum allowed processor load used by the pure model application the minimum computing power required to run the model on a processor with instruction specification according to Table 6.1 is 34.7 kHz for the 10 ms and 34.7 Hz for the 10 s application. Hence research question 2 have been answered.

6.3 Analysis of the EKF and sensor placement consequences

In this section the effect of adding additional sensors are discussed. The most important states to estimate with good accuracy, is the pressure and the liquid volume since these are the only initial states needed to initialize a model simulation as described in 5.2.1. Furthermore the calculation time of the EKF and a simple static observer is computed and improvements for a future embedded vehicular LNG tank observer implantation are suggested. This section hence answers research question 3.

6.3.1 Pressure sensors

It is seen that process noise on the pressure sensor placed in the tank is low in Figure 5-1 and of course this is the optimal sensor placement for the measurement of the tank pressure, since it will always have direct contact with the vapour space of the tank. With this placement the tank pressure p in the state equation 4.28 can be fed to the EKF or to any other observer directly. However such a placement can not replace a sensor in HPP due to diagnosis legislation [15] and also a sensor placed here need to fulfill the requirements of a cryogenic component according to [15]. Any sensor placed before the heat exchanger in the fuel line also need to meet these requirements and will give the tank pressure during vehicle operation with some off-set. After the heat exchanger the difference between the measurements dependant on placement is only the amplitude of the offset and pressure fluctuations, due to varying engine consumption, as seen in Figure 6-1. I.e. elementary the further away from the tank the sensor is placed in the fuel line the more the pressure vary. The offset due to the pressure drop between the tank and the HPP can be incorporated in $h(x, u)$ and the process noise in the HPP can be determined by a comparison between an experimental measurement in the tank and the pressure in the HPP, following the procedure in

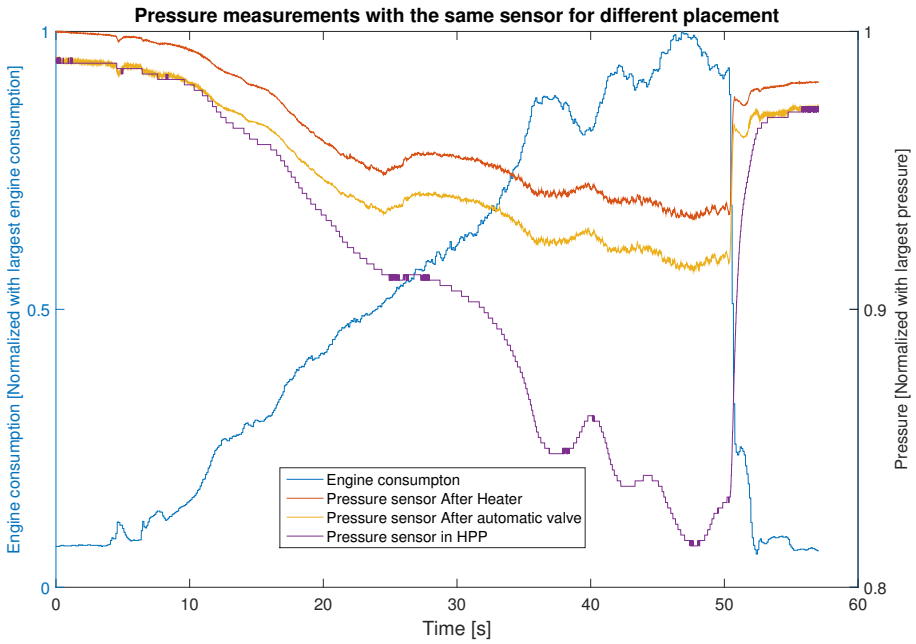

Figure 6-1: Measured pressure variations for different sensor placement in the fuel line after the heat exchanger for a pressure sensor with resolution 0-20 bar. The tank pressure is not measured but it can under such a short and high load be considered almost constant at the highest pressure [3].

section 5.5.4. The sensor noise can be determined from the sensor specification. The results from the prof of concept EKF at light load (Figure 5-16) show that even with 1 bar resolution of the sensor measurement in the HPP and the very slow sample time of 10 s, the EKF can perform like the sensor placed inside the LNG tank. Hence it is concluded that the added production cost with an additional cryogenic approved pressure sensor is not viable since the development cost of implementing an EKF in the long run would be lower. I.e. with an experimental measurement in the tank and a calibrated EKF, the pressure sensor in the HPP can be used as a replacement of the tank pressure sensor and obtain a good result.

6.3.2 Temperature sensor

There exist no temperature sensor in the current system. The purpose of adding one would be to measure the cryogenic liquid temperature and thereby together with the pressure determine the LNG:s deviation from methane. I.e. the more the correspondence between the tank pressure and the LNG temperature deviate from Figure 2-2 the less methane in the mixture. The placement of such a sensor should be in the fuel line as close as possible to the piping exiting the tank seen in Figure 3-1. This so that minimal heating of the cryogenic liquid is done by the fuel line piping in contact with the ambient environment. It should be places in the fuel line and not in the tank for two reasons. 1. The liquid flow over the sensor needs to be sufficient, so that the sensor assumes a temperature as close as possible to the liquid. 2. It is less costly to

add a sensor in the external piping than special order tanks from the manufacturer with an extra temperature sensor since this require an additional certification process for the tank according to [15]. For engine control purposes such as knock control the deviation from methane could be desirable to know. Adding a temperature sensor will also of course enable the EKF to use sensor data to estimate the temperature of the LNG tank better.

6.3.3 Liquid volume sensor

The function of the liquid volume sensor is explained in section 3.4, a better alternative to this solution have not been determined in the thesis since the cryogenic environment in the tank limits the choices. The resolution of the raw voltage sampled from the sensor unit could be increased by a higher resolution ADC conversion. Even though a second reference of measurement is not available to verify the EKF for the liquid volume. The process Q and sensor R noise for the liquid volume can be calibrated to change the behaviour of the EKF estimation of V_l in Figure 5-16. For example if the effect of the tilt of the vehicle on the liquid level is not desired to see Q should be set to a the amplitude of these liquid fluctuations and the EKF will filter this effect away.

6.3.4 Mass sensors

There exist no industrial applicable sensors for measuring mass, only mass flow. This is also measured in the current system as engine consumption and is used in the state space as input as seen in Chapter 4. It is therefore not possible to use sensor data to estimate the mass states in the EKF. Instead the mass states will follow the model purely in any observer implementation.

6.3.5 EKF calculation time

The EKF is computationally heavy due to all of the matrix operations in equations 5.14 and 5.12. Since there exist many different ways to implement matrix operations it is left to the reader to verify the data presented here which is based on the C-code from [32] for the general computation of a matrix inverse, [33][34][35] have the standard practise way to calculate the matrix transpose, the matrix multiplication and the matrix addition in the C-language. With this code, Table 6.1, the central difference (equation 5.16) for computing A and H, equations 5.12 and 5.14, the instructions

required for each step of the EKF algorithm is

$$\begin{aligned} P^-_{k,ins} &= 5377 \\ \hat{x}^-_{k,ins} &= 140 \\ K_{k,ins} &= 5099 \\ \hat{x}_{k,ins} &= 140 \\ P_{k,ins} &= 590 \\ EKF_{ins} &= 11449, \end{aligned} \tag{6.10}$$

note that the model computation is incorporated in these instructions. I.e. the EKF hence require 50 times more instructions than the model. However the matrix inverse code in [32] is far from optimised, for example in many places operations that could have been performed only once are iterated. Since the EKF is only a prof of concept no regard to code execution optimisation of the EKF implementation been taken in the thesis. Therefore it is seen that the implemented numerical central difference of the 5×5 Jacobian A, requires a massive amount of instructions in the computation of P^-_k, which might be possible to reduce through optimization, but is not investigated further in the thesis. Since the inverse in equation 5.14 with the 2 sensor case is a 2×2 matrix a lot of instructions in computing K_k can be eliminated using a 2×2 matrix inverse algorithm. The required instruction for the EKF in equation 6.10 gives a computation time of 143 μs which is a considerable increase when compared to the model. This represent a processor load of 1.43 % on a 10 ms application and $1.4{\cdot}10^{-3}$ % on the 10 s application for which the EKF has been evaluated, against measurement data in section 5.5.4.

Since the model follows the measurement data well in section 5.4.2 implementing the EKF in a real application could be an unnecessary complex solution. An alternative solution is to simply use a calibrated static filter gain K in the state estimate equation 5.14, removing most of the heavy calculations and matrix operation of the EKF. However the dynamic noise compensation for the very noisy tank level sensor and the HPP pressure sensor would be lost. With such an implementation with these sensors, assuming the sample of these are interrupt driven and the calculation to the required units of the sensor value is not done by the model application, i.e. only one load operation per sensor, would require

$$StaticObserver_{ins} = 483$$

instructions. I.e. a computational time of 6.04 μs and a processor load of 0.0604 % for a 10 ms application and 0.6 10^{-4}% for the 10 s application. I.e. still an insignificant processor load with the static observer solution. It is hence concluded that the performance of the static choice should be evaluated before implementing an EKF in a real application, if proven to be sufficient, the static choice should be implemented.

6.3.6 Final remarks EKF

The EKF has been proven to be functional in a 10 s sample time application both at full and light load. The processor load at this application cycle is $1.4{\cdot}10^{-3}$ which is still a very low leaving the vast majority of the embedded system processing power open for safety critical applications and other future control. The sensor placement far away from the cryogenic system is not a problem when using an EKF as shown in section 5.5.4. Also high noise levels are handled well by the EKF by supplying it with the sensor and process noise. The EKF developed in the thesis is a proof of concept, it is hence concluded that the concept works and an EKF can be used as a LNG vehicular tank model observer. The in the thesis suggested implementation can be directly translated to an embedded system and run on a 10 s cyclic EKF application. However it is also concluded and recommended that the implementation code of the EKF should be optimized in order to reduce the instructions required per cycle making the processor load of the EKF lower when running on a lower sample time cyclic application.

Future control will most likely require shorter sample times and hence, require shorter execution time. This despite the slow dynamics of the system, seen in the log data in the model verification Figures in Chapter 5, since according to the rule of thumb for linear control, the sample time should be 10-30 times faster than the fastest pole of the system. Furthermore when more measurements have been performed on the LNG vehicular tank, the process noise q should be calibrated to more reliable values for each state before an implementation. Analogously the sensor noise r should be determined once the sensors to be used by the EKF has been determined. The recommendation based on the thesis results and the developed models implementation, is that the sensors to be used by the EKF is the HPP pressure sensor and the liquid level sensor. If it is determined that the composition of the LNG strongly affect the engine combustion cycle it is also suggested that a temperature sensor in the fuel line, as close as possible to the outlet of the tank, is added to the system, incorporated in the EKF implementation and that LNG composition determination functionality is incorporated in the model.

The EKF is a very complex, computationally heavy, dynamical observer and it is seen in section 6.3.5, that it require far more instructions per cycle than the static choice. Only the EKF dynamical observer have been evaluated at light load with the sensors intended for the implementation, at 10 s application cycle time were it performs fair when liquid is extracted from the tank and at 1 s application cycle time where it performs well during the whole measurement. At a 10 ms cyclic application the EKF only has a processor load of 1.4 % which would not lock the processor from performing safety critical tasks and is just barley larger than the processor load that research question 4 is concerned with for only computation of the model. Like mentioned in section 6.1.3 since the intended model implementation uses only two sensors for both the initialization and the observer, it is sensitive to error in these measurements. In this sense the higher processor load of a dynamic EKF could be

motivated by the low amount of sensors used by the complete model application and with this ensuring the correct estimation of the tank pressure and liquid volume and thereby ensuring correct estimation of all tank states. However before implementing such a solution at the least also the liquid volume state should be verified against a second measurement reference and if possible all states of the tank. The high processor load of the EKF could furthermore be motivated with the usage of a lower accuracy tank model as discussed in section 6.1.4 i.e. a shorter computational time of the model would also reduce the computational time of the EKF. Based on that the model uncertainty is known and that the EKF can estimate the states with this knowledge. In section 6.3.5 it is shown that a static gain observer has a very low processor load for both the 10ms and 10 s application. I.e. since research question 3 is only concerned with what is possible it can be answered with; both observers are possible to use and the possible sensors and placement is the one in sections 6.3.1-6.3.4.

Bibliography

[1] W.C.Reynolds: Thermodynamic properties in SI. R50. http://christophe.lauverjat.pagesperso-orange.fr/mava/images/F_R50_(Methane).gif. Accessed 2015-05-25.

[2] P.J. Linstrom and W.G. Mallard. *NIST Chemistry WebBook, NIST Standard Reference Database*, volume 69. National Institute of Standards and Technology, Gaithersburg MD, 20899. http://webbook.nist.gov/cgi/fluid.cgi?PLow=0.1&PHigh=20&PInc=0.000001&Applet=on&Digits=5&ID=C74828&Action=Load&Type=SatT&TUnit=K&PUnit=MPa&DUnit=kg\%2Fm3&HUnit=kJ\%2Fkg&WUnit=m\%2Fs&VisUnit=uPa*s&STUnit=N\%2Fm&RefState=DEF accessed 2015-05-12.

[3] MATLAB. *version MATLAB 8.2 (R2013b)*. The MathWorks Inc., Natick, Massachusetts, 2013.

[4] Q.-S Chen, J Wegrzyn, and V Prasad. Analysis of temperature and pressure changes in liquefied natural gas (lng) cryogenic tanks. *Cryogenics*, 44(10):701 – 709, 2004.

[5] Cryogenic Fuels Inc. Liquid methane fuel characterization and safety assessment report. *Report No. CFI-1600*, December 1991.

[6] Chart industries. *LNG Vehicle Fuel Tank System Operation Manual*. Chart industries, lng@chartindustries.com.

[7] Freescale Semiconductor. *e200z6 PowerPC Core Reference Manual*. Freescale Semiconductor, support@freescale.com.

[8] Aldo Bassi. Liquefied natural gas (lng) as fuel for road heavy duty vehicles technologies and standardization. In *SAE Technical Paper*. SAE International, 09 2011.

[9] Nils Olof Nylund, Veikko Karvonen, Hannu Kuutti, and Juhani Laurikko. Comparison of diesel and natural gas bus performance. In *SAE Technical Paper*. SAE International, 09 2014.

[10] Rapid calculation procedure to determine the pressurizing period for stored cryogenic fluids. *Applied Thermal Engineering*, 30(1415):1997, 2010.

[11] J.D Murphy, E McKeogh, and G Kiely. Technical/economic/environmental analysis of biogas utilisation. *Applied Energy*, 77(4):424,425, 2004.

[12] Lionel Perrette and Helmut K. Wiedemann. Safe storage of natural gas on urban buses: Case early investigation and learnings. In *SAE Technical Paper*. SAE International, 04 2007.

[13] Klaus D Timmerhaus and Richard Reed. *Cryogenic engineering: fifty years of progress*. Springer Science & Business Media, University of Colorado Boulder, CO 80305 Boulder, CO 80309 USA, 2007.

[14] V.F Getmanets, L.G Goncharenko, R.S Mikhalchenko, N.P Pershin, G.G Zhun, and H Stears. The single component superinsulation. *Cryogenics*, 39(12):1037 – 1038, 1999.

[15] Economic Commission for Europe Inland Transport Committee. Proposal for supplement 1 to the 01 series of amendments to regulation no. 110 (cng vehicles). World Forum for Harmonization of Vehicle Regulations 161st session Geneva, November 2013.

[16] Y. Chen, Z. Tang, and J. Yu. Using multi-sensor data fusion to predict dangerous states of lng transport tank. pages 278–280, 2012. cited By 0.

[17] CCE Center for Energy Economics. Composition of natural gas and lng. `http://www.beg.utexas.edu/energyecon/lng/LNG_introduction_07.php`. Accessed 2015-05-05.

[18] George Karavalakis, Maryam Hajbabaei, Thomas Durbin, Zhongqing Zheng, and Kent Johnson. Influence of different natural gas blends on the regulated emissions, particle number and size distribution emissions from a refuse hauler truck. *SAE Int. J. Fuels Lubr.*, 5:928–944, 09 2012.

[19] Prof. Z. S. Spakovszky. Thermodynamics and propulsion 8.1 behavior of two-phase systems. `http://web.mit.edu/16.unified/www/FALL/thermodynamics/notes/node61.html`. Accessed 2015-05-03.

[20] Prof. Z. S. Spakovszky. Thermodynamics and propulsion 8.2 work and heat transfer with two-phase media. `http://web.mit.edu/16.unified/www/FALL/thermodynamics/notes/node62.html`. Accessed 2015-05-07.

[21] Prof. Z. S. Spakovszky. Thermodynamics and propulsion 2.4 specific heats: the relation between temperature change and heat. `http://web.mit.edu/16.unified/www/FALL/thermodynamics/notes/node18.html`. Accessed 2015-05-07.

[22] Hans Havtun. *Applied Thermodynamics - Collection of Formulas*. Thermal Engineering E&R, thermal.engineering@havtun.se, 2012.

[23] Ph. Lebrun and L. Tavian. 8.3 cryogenics. In *Accelerators and Colliders*, pages 8.3–8, 8.3–9. Springer-Verlag GmbH, Heidelberg, 2013.

[24] X.Ji E.Adom, S.Z.Islam. Modelling of boil-off gas in lng tanks a case study. *International Journal of Engineering and Technology*, 2(4), 2010.

[25] Cryostar 2009. Lng/lcng vehicle refuelling stations. `http://www.cryostar.com/web/lcng-lng-filling-stations.php`. Accessed 2015-05-02.

[26] Manson Benedict, George B. Webb, and Louis C. Rubin. An empirical equation for thermodynamic properties of light hydrocarbons and their mixtures ii. mixtures of methane, ethane, propane, and nbutane. *The Journal of Chemical Physics*, 10(12), 1942.

[27] ZHANG Juyong LI Rong, LI Tuo. Study on vehicular lng tank. *Applied Mechanics & Materials*, 687-691:175–178, 2014.

[28] Rama Subba Reddy Gorla. Probabilistic analysis of a liquefied natural gas storage tank. *Applied Thermal Engineering*, 30(1718):2763 – 2769, 2010.

[29] Greg Welch and Gary Bishop. *An Introduction to the Kalman Filter*. Department of Computer Science University of North Carolina., Chapel Hill, NC 27599-3175, 2013.

[30] Erik Hōckerdal. *Model Error Compensation in ODE and DAE Estimators with Automotive Engine Applications*. PhD dissertation, Linkōping University, Division of Vehicular Systems, Department of Electrical Engineering, Linkping University, SE581 83 Linkping, Sweden.

[31] Svante Lothgren Erik Klingborg Christian Wessel, Marten Wallengren. A method and a system for determining time data relating to a non-combustion outlet process of a fuel gas from a gas tank at a vehicle, 1551604-0, 2015-12-08.

[32] Jason Yu-Tseh Chi. Calculation of matrix inverse in c/c++. `https://chi3x10.wordpress.com/2008/05/28/calculate-matrix-inversion-in-c/`. Accessed 2015-05-23.

[33] Programming Simplified. C program to transpose a matrix. `http://www.programmingsimplified.com/c-program-transpose-matrix`. Accessed 2015-05-23.

[34] Programming Simplified. Matrix multiplication in c. `http://www.programmingsimplified.com/c-program-multiply-matrices`. Accessed 2015-05-23.

[35] Programming Simplified. C program to add two matrix. `http://www.programmingsimplified.com/c-program-add-matrices`. Accessed 2015-05-23.